

Application of Continuous Ramped Heating to Assess Dispersion in Apatite (U-Th)/He Ages: A case study from Transantarctic Mountains of southern Victoria Land

Hongcheng Guo¹, Peter Zeitler¹, Bruce Idleman¹, Annia Fayon², Paul Fitzgerald³, and Kalin McDannell⁴

¹Lehigh University

²University of Minnesota

³Syracuse University

⁴Dartmouth College

November 26, 2022

Abstract

Application of apatite (U-Th)/He thermochronology has been hindered by incomplete understanding of single-grain age dispersion often displayed by samples, particularly those from older, slowly cooled settings. To assess the capability of continuous ramped heating (CRH) to explain dispersion, we performed a study on an apatite suite from Cathedral Rocks in the Transantarctic Mountains (TAM) that have high age dispersion. Examining 132 apatite grains from a total of six samples, we confirmed earlier apatite (U-Th)/He results showing that measured AHe ages have at least three-fold intra-sample dispersion with no obvious relationships between ages and effective uranium concentration (eU) or grain size. CRH results on these apatites yielded two groups. Those with younger ages, characterized by single-peak incremental 4He gas-release curves, displayed simple volume diffusion behavior. In contrast, grains with older ages generally show anomalous gas release in the form of sharp spikes and / or extended gas-release at high temperatures (i.e., ≥ 800 °C). Well-behaved apatites still show considerable age dispersion that exceeds what grain size, radiation damage, and analytical uncertainty can explain, but this dispersion appears to be related to variations in 4He diffusion kinetics. The screened AHe ages from well-behaved younger apatite grains together with kinetic information from these grains suggest that the sampled region experienced slow cooling prior to rapid cooling (rock exhumation) beginning ca. 35 Ma. This interpretation is consistent with other studies indicative of an increase in exhumation rates at this time, possibly related to the initiation of glaciation at the Eocene-Oligocene climate transition. An attempt to correct anomalous older apatite ages by simply removing extraneous gas-release components is proposed yielded some ages that are too young for the samples' geologic setting, suggesting that the factors that lead to anomalous laboratory release behavior can impact both the expected radiogenic component as well as those that are extraneous. From our observations we conclude that: (1) CRH analysis can serve as a routine screening tool for AHe dating and offers opportunities to reveal first-order kinetic variations; (2) model-dependent age correction may be possible but would require some means of estimating the broad proportions of 4He components incorporated into grains before and after closure to diffusion, and (3) interpretation of highly dispersed AHe ages requires assessment of individual-grain diffusion kinetics beyond that predicted by radiation-damage models. We also infer that many apatite grains contain imperfections of varying kinds that contribute significantly to kinetic variability beyond that associated with radiation damage.

1 **Application of Continuous Ramped Heating to Assess Dispersion in Apatite (U-**
2 **Th)/He Ages: A case study from Transantarctic Mountains of southern Victoria**
3 **Land**

4 Hongcheng Guo^{a,*}, Peter K. Zeitler^a, Bruce D. Idleman^a, Annia K. Fayon^b, Paul G.
5 Fitzgerald^c, Kalin T. McDannell^d

6
7 ^aDepartment of Earth and Environmental Sciences, Lehigh University, Bethlehem, PA 18015

8 ^bDepartment of Earth Sciences, University of Minnesota, Minneapolis, MN 55455

9 ^cDepartment of Earth and Environmental Sciences, Syracuse University, Syracuse, NY 13244

10 ^dDepartment of Earth Sciences, Dartmouth College, Hanover, NH 03755

11 * Corresponding author: Hongcheng Guo (hog217@lehigh.edu)

12 *Keywords:* Apatite; (U-Th)/He; Thermochronology; Age Dispersion; Helium; Diffusion;
13 Transantarctic Mountains

14 **ABSTRACT**

15 Application of apatite (U-Th)/He thermochronology has been hindered by incomplete
16 understanding of single-grain age dispersion often displayed by samples, particularly
17 those from older, slowly cooled settings. To assess the capability of continuous ramped
18 heating (CRH) to explain dispersion, we performed a study on an apatite suite from
19 Cathedral Rocks in the Transantarctic Mountains (TAM) that have high age dispersion.
20 Examining 132 apatite grains from a total of six samples, we confirmed earlier apatite (U-
21 Th)/He results showing that measured AHe ages have at least three-fold intra-sample
22 dispersion with no obvious relationships between ages and effective uranium
23 concentration (eU) or grain size. CRH results on these apatites yielded two groups. Those
24 with younger ages, characterized by single-peak incremental ⁴He gas-release curves,
25 displayed simple volume diffusion behavior. In contrast, grains with older ages generally
26 show anomalous gas release in the form of sharp spikes and / or extended gas-release
27 at high temperatures (i.e., ≥ 800 °C). Well-behaved apatites still show considerable age
28 dispersion that exceeds what grain size, radiation damage, and analytical uncertainty can
29 explain, but this dispersion appears to be related to variations in ⁴He diffusion kinetics.
30 The screened AHe ages from well-behaved younger apatite grains together with kinetic
31 information from these grains suggest that the sampled region experienced slow cooling
32 prior to rapid cooling (rock exhumation) beginning *ca.* 35 Ma. This interpretation is
33 consistent with other studies indicative of an increase in exhumation rates at this time,
34 possibly related to the initiation of glaciation at the Eocene-Oligocene climate transition.
35 An attempt to correct anomalous older apatite ages by simply removing extraneous gas-
36 release components is proposed yielded some ages that are too young for the samples'
37 geologic setting, suggesting that the factors that lead to anomalous laboratory release
38 behavior can impact both the expected radiogenic component as well as those that are
39 extraneous. From our observations we conclude that: (1) CRH analysis can serve as a
40 routine screening tool for AHe dating and offers opportunities to reveal first-order kinetic
41 variations; (2) model-dependent age correction may be possible but would require some

42 means of estimating the broad proportions of ^4He components incorporated into grains
43 before and after closure to diffusion, and (3) interpretation of highly dispersed AHe ages
44 requires assessment of individual-grain diffusion kinetics beyond that predicted by
45 radiation-damage models. We also infer that many apatite grains contain imperfections
46 of varying kinds that contribute significantly to kinetic variability beyond that associated
47 with radiation damage.

48 **1. Introduction**

49 Following the proposal that apatite (U-Th)/He (AHe) ages could be used as a low-
50 temperature thermochronometer (Zeitler, 1987), advances in pursuing the fundamental
51 diffusion systematics and kinetics of helium release (Wolf et al., 1996; Farley et al., 1996;
52 Farley, 2000; Shuster et al., 2006; Flowers et al., 2009) has led apatite (U-Th)/He
53 thermochronology to become widely used in studies of tectonic and surface processes
54 (e.g., Reiners et al., 2003; Ehlers and Reiners, 2005; Fitzgerald et al., 2006; Flowers and
55 Farley, 2012; Toraman et al., 2014; Long et al., 2015). However, it has become widely
56 recognized that interpretation of AHe data is often complicated by intra-sample age
57 variations (commonly referred as “excess age dispersion”) that are beyond typical
58 analytical uncertainties (e.g., Fitzgerald et al., 2006; Flowers and Kelley, 2011; Peyton et
59 al., 2012; Zeitler et al., 2017; McDannell et al., 2018). Significant efforts have been made
60 to explain such age dispersion and to unravel complexities in ^4He diffusion systematics.
61 Some factors, for example the presence of U-rich micro-inclusions (Farley, 2002), U and
62 Th zonation (Meesters and Dunai, 2002, Fitzgerald et al., 2006), and ^4He implantation
63 (Spiegel et al., 2009, Murray et al., 2014) will complicate He analysis or diffusion
64 systematics in ways that make it difficult to obtain useful apparent ages (Farley, 2000).
65 Other effects such as grain size (Reiners and Farley, 2001), broken grains, (Beucher et
66 al., 2013; Brown et al., 2013) and the way that radiation damage systematically alters He
67 diffusion kinetics (Shuster et al., 2006; Gautheron et al., 2009; Flowers et al., 2009; Willett

68 et al., 2017) can lead to age dispersion that can be exploited to reveal more information
69 about thermal history. Slow cooling through or long-term residence within an apatite (U-
70 Th)/He partial retention zone will accentuate age dispersion, often to a considerable
71 degree (e.g., Reiners and Farley 2001; Fitzgerald et al., 2006).

72 Despite these contributions, there are still situations where we still cannot fully explain
73 commonly observed AHe age dispersion. Applied studies of sample suites from different
74 geologic settings have found that even using careful sample selection, grain size and
75 radiation damage can only explain some of the observed dispersion (Zeitler et al., 2017).
76 To reduce the probability of overdispersed ages and to understand age dispersion should
77 this occur, common practices include performing “re-extracts” to evaluate if all He has
78 been out-gassed, collecting data only from single-grains, performing large-n replicate
79 analyses, and plotting He ages vs. size (radius) and effective uranium [eU] to evaluate
80 excess dispersion. If excess dispersion occurs, complex data sets can be vexing and
81 difficult to interpret and use in thermal history modeling, and if a large number of samples
82 and single-grain analyses are undertaken in order to circumvent such issues, these
83 approaches are time-consuming and costly.

84 As a result, the thermochronology community is actively working on the challenge that
85 excess age dispersion presents (e.g., Zeitler et al., 2017; McDannell et al. 2018). A
86 possible factor in age dispersion that has attracted recent attention is the role that crystal
87 imperfections of various types can play in changing diffusion behavior (Djimbi et al., 2015;
88 Fayon and Hansen, 2015; Gerin et al., 2017; Zeitler et al., 2017), adding to the impact
89 that imperfections associated with radiation damage have on diffusion kinetics. This focus

90 is not a new concept, as Farley (2000) argued that *“Regardless of model, a critical*
91 *question for apatite helium thermochronometry is whether the total abundance of defects*
92 *affects the helium retentivity in the low temperature regime and, if so, how and when the*
93 *defects are acquired.”*

94 Here, we use a recently developed analytical approach, continuous ramped heating
95 (hereafter, CRH, Idleman et al., 2018) which is described in **section 2.2**, to assess this
96 long-standing problem of excess AHe age dispersion by closely examining samples from
97 a well-characterized geological setting. In a broad survey of natural samples, McDannell
98 et al. (2018) suggested that CRH should be able to identify variable ^4He outgassing
99 behavior in the form of differing gas-release components. Our work aims to test this
100 suggestion using a classic sample suite (Fitzgerald et al., 2006) from the Ferrar Glacier
101 area of southern Victoria Land in Transantarctic Mountains that yielded highly dispersed
102 AHe ages (section 2.1). We seek to better document how CRH can reveal relationships
103 between AHe ages and ^4He outgassing behavior such that it can be deployed as a routine
104 sample-characterization tool to extract interpretable data from complex sample sets.

105 **2. Study Material and Analytical Methods**

106 **2.1. The Transantarctic Mountain apatite suite**

107 Ideal apatite samples for our study should (1) have significant dispersed AHe ages, which
108 is not uncommon, but also (2) carry other thermochronologically and geologically
109 constrained thermal history (i.e., rock cooling history; local or regional geological events)
110 to allow assessment and interpretation of dispersed data, which is challenging. The
111 Transantarctic Mountains are a good locality to test our questions because their tectonic

112 and thermochronological setting is well established and their overall history of slow
113 cooling since the Mesozoic will tend to amplify any dispersion in AHe ages which may be
114 due to variations in ^4He diffusion systematics. We have selected a vertical profile collected
115 from basement granitoids in the Ferrar Glacier area of southern Victoria Land in the
116 Transantarctic Mountains – Cathedral Rocks – because of its thermal history, as well as
117 the availability of both AHe and apatite fission track (hereafter, AFT) age constraints from
118 previous studies (e.g., Fitzgerald et al. 1992; 2002). Those studies suggest the locality
119 also experienced relatively rapid cooling early in the Oligocene, possibly resulting from
120 the onset of glacial incision or a change in tectonics.

121 The Transantarctic Mountains (**Fig. 1**) have long been regarded as an intriguing feature
122 owing to their large size (>2500 km long), high elevations (>4 km) and the way they define
123 the western flank of the West Antarctic rift system, in essence separating the significantly
124 different geological terranes of East and West Antarctica (e.g., Dalziel 1992, Fitzgerald,
125 2002, Goodge 2020). The West Antarctic rift system underwent two phases of extension,
126 early initiation in the middle Mesozoic (e.g., Elliot and Fleming, 2004), and then a later
127 post-Eocene phase (e.g., Wilson et al., 1998; Florindo et al., 2001; Smellie, 2001). In
128 many locations along the TAM including the Ferrar Glacier region, the mountains have a
129 layer-cake stratigraphy that dips ($1\text{-}2^\circ$) gently inland before disappearing under the East
130 Antarctica Ice Sheet (e.g., Gunn and Warren 1962; Goodge 2002). In southern Victoria
131 Land basement rock is dominated by the arc-related Cambro-Ordovician magmatic suite
132 of the Granite Harbour Intrusives (e.g., Allibone et al. 1993) intruded into polydeformed
133 metasedimentary rocks (e.g., Goodge 2020) during the Ross Orogeny. Devonian to
134 Triassic flat-lying sedimentary rocks known as the Beacon Supergroup were then

135 deposited unconformably on a basement erosion surface. Basin sedimentation was
136 subsequently ended by extensive basaltic flood magmatism marking the breakup of
137 Gondwana, expressed in southern Victoria Land as the Ferrar Dolerite, presenting as
138 thick (~300 m) sills within basement, and along the unconformity, as well as thinner sills
139 distributed within Beacon sediments (e.g., Gunn and Warren 1962). Subsequent to Ferrar
140 magmatism, the TAM was formed largely related to uplift along the West Antarctic rift
141 flank (e.g., Fitzgerald 1992).

142 There is a rich collection of thermochronology studies in southern Victoria Land, both
143 onshore (Gleadow et al., 1984; Gleadow and Fitzgerald, 1987; Fitzgerald and Gleadow,
144 1988; Fitzgerald 1992, 2002; Olivetti et al., 2018) and offshore (Fitzgerald 2001, Olivetti
145 et al., 2013) that generally indicate episodic exhumation with periods of enhanced cooling
146 and exhumation (though slow relative to most active orogens) in the Cretaceous and
147 Cenozoic. Fitzgerald et al. (2006) sought to explore the younger part (less than ca. 50
148 Ma) of the exhumation history by integrating AFT data with inverse thermal models,
149 combined with, what at that time, was the relatively new approach of apatite (U-Th)/He
150 dating. However, apatite (U-Th)/He ages from two vertical profiles collected on either side
151 of the Ferrar Glacier displayed considerable single-grain age variation (**Fig. 1**). Thus, the
152 focus of that study shifted from constraining the younger exhumation history of the TAM
153 towards documenting and exploring why over-dispersion occurs and how such data might
154 be interpreted. Nevertheless, constraints on the cooling and exhumation history of this
155 part of the TAM were obtained. With less AHe age dispersion within data from the north
156 side vertical profile (Peak 1880) the interpretation was more complete: slow cooling
157 (exhumation) from Late Cretaceous to early Eocene (~1°C/Myr), an increase at ca. 43

158 Ma, slowing again until an increase in the late Eocene (ca 37–35 Ma). On the south side
159 of the glacier AHe data from a vertical profile from the eastern-most of the peaks of the
160 Cathedral Rocks had much greater age dispersion than the Peak 1880 profile, thus the
161 interpretation relied mainly on AFT data/models and the AHe ages added very little to our
162 understanding of the younger cooling history. At Cathedral Rocks, the interpretation was
163 that cooling/exhumation was relatively slow ($\sim 1^\circ\text{C}/\text{Myr}$) from Cretaceous to the early
164 Cenozoic with slightly faster cooling/exhumation beginning ca. 50 Ma ($\sim 2.8^\circ\text{C}/\text{Myr}$).

165 For CRH screening and AHe dating, apatite grains were selected from six samples from
166 the Ferrar Glacier profile at Cathedral Rocks, originally labeled R22641, R22642, R22643,
167 R22644, R22645, R22646 from high to low elevation (Fitzgerald et al., 2006). To simplify
168 communication, we renamed them R1, R2, R3, R4, R5, R6, respectively, in the following
169 discussion. All apatite grains were picked, examined, and photographed using a Nikon
170 SMZ800 microscope under plain light at $\sim 95\times$ magnification for optical characterization
171 to determine shape and size for calculation of alpha-ejection correction factors and to
172 assess basic grain characteristics such as presences of crystal imperfections such as
173 inclusions, euhedral-vs-anhedral shape, and grain integrity (see **Research Data – Table**
174 **A1**).

175 **2.2 Sample Characterization**

176 **2.2.1 Chemistry**

177 To document their overall composition as well as variability, we analyzed a number of
178 grains from two samples (R1 and R2) by electron microprobe. Complete results are found
179 in the online archive; Table 1 summarizes results by averaging data for all spots for all

180 grains. Only Si, Ce, and F show some modest scatter, but Si and Ce are present at low
 181 concentrations. The grains are all fluorapatite in composition, with an average proportion
 182 for Fap:Cap:Hap (Piccoli and Candela, 2002) of 0.859 : 0.007 : 0.133 . Values of the
 183 fission-track annealing parameter *rmr0* (Ketcham et al., 2007) calculated from the
 184 elemental analyses range from 0.829 to 0.840, signifying near endmember fluorapatite
 185 (**Appendix A – Fig. A.1**).

	TAMR1 N=48 spots, 30 grains				TAMR2 N=51 spots, 30 grains			
	Mean	SD	CDL99	MSWD	Mean	SD	CDL99	MSWD
Si	0.126	0.051	0.006	188	0.150	0.056	0.010	200
Y	0.121	0.053	0.030	7.2	0.151	0.057	0.030	8.4
La	<i>0.044</i>	<i>0.031</i>	0.031	4.3	<i>0.035</i>	<i>0.028</i>	<i>0.030</i>	3.6
Ce	0.195	0.060	0.029	15.4	0.204	0.071	0.030	22.1
Mg	<i>0.003</i>	<i>0.003</i>	0.006	1.0	<i>0.008</i>	<i>0.015</i>	<i>0.010</i>	1.7
Ca	39.63	0.159	0.010	3.7	39.47	0.222	0.010	9.3
Sr	<i>0.014</i>	<i>0.007</i>	0.013	1.1	<i>0.014</i>	<i>0.008</i>	<i>0.010</i>	1.6
Na	<i>0.010</i>	<i>0.007</i>	0.009	2.2	<i>0.012</i>	<i>0.009</i>	<i>0.010</i>	2.2
P	18.53	0.139	0.014	2.0	18.44	0.125	0.010	1.8
S	<i>0.001</i>	<i>0.002</i>	0.006	0.8	<i>0.001</i>	<i>0.003</i>	<i>0.010</i>	1.0
Cl	0.059	0.027	0.009	13.0	0.043	0.023	0.010	3.3
F	3.179	0.203	0.032	54.0	3.290	0.197	0.030	48.0
O	38.62	0.15			38.44	0.16		
TOTAL	100.53	0.36			100.25	0.42		

186 **Table 1.** Electron microprobe analyses of apatites from two TAM samples. Means,
 187 standard deviations, and detection limits are in weight percent. MSWD (mean square of
 188 weighted deviates) serves as measure of scatter of values relative to instrument
 189 uncertainties. Values in italics are near or below detection limit.

190 2.2.2 Survey of crystallographic defects

191 We examined polished sections of grains from samples R1 and R2 to assess the
 192 prevalence of defects in TAM apatites. Before polishing, grains were annealed at 500 °C
 193 for 60 minutes to remove any fission tracks, and then etched using two different solutions,

194 a typical 5M HNO₃ solution commonly used for fission-track etching, and also a 0.5 M
195 HNO₃ solution to focus on smaller more delicate structures. Detailed from this work are
196 part of an ongoing study, but for this paper the key observation is that TAM apatite grains
197 are highly variable in defect density, ranging from nearly imperfection-free to being riddled
198 with imperfections of various types (**Fig. 2**).

199 **2.3 Data collection and analysis**

200 Individual grains were placed in closed niobium tubes, degassed of their ⁴He via the CRH
201 method at the Lehigh University noble-gas geochronology lab (see below and **Appendix**
202 **B** for details), and measured for parent U-Th-Sm isotopes via dissolution and isotope
203 dilution at the Arizona Radiogenic Dating Laboratory with detailed procedures reported
204 by Reiners and Nicolescu (2006).

205 **2.3.1 Continuous ramped heating**

206 The CRH method characterizes the diffusive loss of ⁴He by continuous heating following
207 a progressively increasing temperature schedule, typically at a fixed rate. Evolved He is
208 measured continuously as a function of time and temperature (Idleman et al., 2018). Our
209 early experiments (Idleman et al., 2018; McDannell et al., 2018) used a resistance furnace
210 for heating, which we have now replaced with a fiber-coupled diode laser system. The
211 laser provides more precise time and temperature control, less temperature lag (i.e.,
212 better response time), and lower loads of potentially interfering active gases coevolved
213 with He. Here we briefly outline the most recent analytical procedure of our
214 implementation of CRH and include a complete documentation of this CRH procedure in
215 **Appendix B**. We also provide our observations made on the behavior of standard

216 Durango apatite to document the behavior of simple ^4He diffusion systematics as
217 measured by our newest application of the CRH method.

218 **2.3.2 Sample handling**

219 After being selected and photographed, each apatite grain was placed in a closed clean
220 niobium (Nb) tube, which had been cleaned and degassed for 3 hours in a vacuum
221 furnace at 600 °C. The tube was then placed in a hand-made Nb foil envelope ~4 mm in
222 diameter that had also been prewashed and degassed. We used these small envelopes
223 to present an even, flat surface to the laser beam in order to achieve better temperature
224 control and measurement. The packages were placed in quartz-glass holders located in
225 a mobile sample rack that allows us to load multiple samples and analyze them without
226 breaking vacuum.

227 **2.3.3 Data collection**

228 Each CRH run was performed under static vacuum conditions with the mass
229 spectrometer directly open to the sample cell. At the beginning of an analysis, the
230 extraction line was isolated from its pumping system and the ^4He beam was measured
231 and recorded for 3 – 4 minutes, allowing us to estimate cold-blank accumulation rates
232 before the initiation of heating. After heating began, temperatures were recorded by an
233 optical pyrometer capable of measurement over a range of ~180 to >1200°C. Peaks at
234 masses 1, 2, 3, 4, and 28 were measured and recorded continuously using a Balzer
235 Prisma Plus quadrupole mass spectrometer. Besides ^4He , the peaks corresponding to H,
236 H_2 , HD, and N_2 were monitored because we have found that in some runs at high levels
237 these active gases can have a moderate impact on ^4He sensitivity by attenuating the

238 mass 4 beam at temperatures greater than 850 to 900 °C. Two SAES GP50 getter pumps
239 (operated at 20°C and 200°C) were used to reduce the partial pressures of these active
240 gases during analysis so that their effects on ⁴He were never more than a few percent at
241 high temperatures, when hydrogen and nitrogen attain their highest levels (up to 100x
242 those at seen in the cold background signal).

243 All samples were heated to a temperature of at least 800°C. Samples that continued to
244 outgas ⁴He at 800°C were heated further until they showed no additional ⁴He contribution
245 for at least 1 minute, or until they reached 1100°C (whichever came first). After allowing
246 2-3 minutes for sample cool-down and additional purification of the evolved ⁴He, a
247 metered aliquot of about ⁴He of 2.22×10^{-13} mol was introduced to allow determination of
248 the total ⁴He by the method of standard additions. In some cases, this post-run cleanup
249 step was preceded by a small increase in the total-release ⁴He signal (rarely exceeding
250 5%), reflecting gettering of the active gas species suppressing ⁴He sensitivity. This small
251 suppression does not have a significant impact on relative patterns of CRH release
252 behavior but is clearly important to eliminate before measuring the final ⁴He abundance
253 for accurate age determination.

254 **2.3.4 Data reduction**

255 During our CRH runs for the Cathedral Rocks apatites, individual crystals were heated at
256 a fixed rate of 30°C/minute, and temperature and ⁴He measurements were recorded
257 every 10 seconds. To smooth noise in the measured sample temperatures, particularly
258 at low temperatures, we performed a rolling 11-point linear regression of the measured
259 temperatures and registered the times of ⁴He measurement blocks with the regressed

260 temperature record through interpolation. In practice, sample temperatures determined in
261 this way agree with the targeted setpoint temperatures defined by the heating schedule
262 to within 2-3°C. The ^4He beam values were then corrected for dynamic background and
263 evolved blank, yielding final CRH results in the form of tables of time, temperature, and
264 corrected ^4He beam values. From these results we calculated the first derivative of
265 fractional loss (f) to construct incremental ^4He loss curves (df/dT vs T , hereafter df as
266 shorthand) and extract kinetic data ($\ln(D/a^2)$, $(1/s)$, and $10000/T$ (K)) for each sample.
267 These data are available in the data repository as **Table A2** and **Table A3**.

268 **2.3.5 Expected behavior: Durango apatite**

269 We carried out CRH analyses of Durango apatite, an apatite standard widely used by the
270 thermochronology community known for its reproducibility in AHe age (McDowell et al.,
271 2005) and ^4He diffusion kinetics (Farley, 2000) with two goals: using its degassing
272 behavior as a benchmark for expected CRH gas-release patterns and using its kinetics
273 to test analytical reproducibility. We performed CRH screening on both internal fragments
274 and abraded balls that were made from air abrasion experiments using an apparatus
275 similar to that described by Krogh (1982).

276 The spherical-equivalent radii (Ketcham et al., 2011) of our grains ranged from 99 to 118
277 μm for the shards and from 90 to 167 μm for the balls. In general, df curves for both the
278 shards and balls (**Fig. 3A**) exhibit the simple, consistent unimodal peaks predicted by
279 volume diffusion theory (see modeled ^4He outgassing behavior via volume diffusion under
280 CRH in Idleman et al., 2018 and McDannell et al., 2018). We intentionally include results
281 from balls with varying radius to show the precision of our CRH temperature control. With

282 the same heating schedule of 30°C/min, the larger grains show a slightly higher-
283 temperature peak-gas release (McDannell et al., 2018) compared to medium-sized balls
284 (**Fig. 3A**), and the peak-gas release occurred at lower temperatures for one of the
285 smallest balls despite some moderate roughness.

286 This size-controlled kinetic variability is also evident on the Arrhenius plot (**Fig. 3B**) where
287 these grains overall show similar behavior but with offsets from published kinetics by
288 different extents that generally reflect their sizes. After recasting all the results to the same
289 radius (80 µm, **Fig. 3C**), we effectively removed the effect of grain size. Because the
290 estimated spherical-equivalent radii of the balls are far more accurate and consistent than
291 that of the shards, we use the remaining kinetics variation within these balls as an
292 estimate of temperature uncertainty. At observed values of $\ln(D/a^2)$ of -14 and -12 1/s,
293 the measured temperature ranges for the size-corrected data are 310.5 ± 8.0 °C and
294 375.1 ± 7.8 °C, respectively, consistent with the variation we observe when we perform
295 calibration of the optical pyrometer against a reference thermocouple.

296 **2.3 Technical issues**

297 Using affordable hardware, a single CRH analysis can be done quickly in about the same
298 time as a conventional He analysis, and so represents a potentially routine screening tool
299 that every thermochronology laboratory can perform. There are a few technical issues
300 that are important to appreciate in order to fully understanding the data from this study.
301 These technical concerns have implications for measurement of low-temperature kinetics
302 (**Fig. 3B, C; Fig. 8**) and for overall data precision.

303 The major challenge when undertaking CRH experiments is temperature measurement,
304 especially in the low-temperature regime (i.e., < 250°C). To increase sample throughput,
305 we measure temperature for each grain using an optical pyrometer rather than a
306 thermocouple. The pyrometer is calibrated with a thermocouple-instrumented sample
307 packet each day before CRH runs. However, two difficulties prevented us from obtaining
308 a robust temperature measurement below ~300°C. First, at the time of sample analysis,
309 our pyrometer had a lower temperature limit of ~198°C. Second, due to the time needed
310 for a sample package to reach thermal equilibrium at low temperatures we often observed
311 (1) temperatures recorded from the pyrometer that were lower than that from the
312 reference thermocouple right after laser startup until ~300 °C and (2) spikes of higher-
313 than-expected temperature readings (laser overshooting) during this time period. The net
314 apparent effect seems mostly to be lower-than-expected ⁴He release at low temperatures
315 that created significant non-linear trends in Arrhenius plots of Durango apatites (**Fig. 3B,**
316 **C**), which have been shown to give linear trends during long heating experiments at low
317 temperatures (Farley, 2000). We call out this issue because even after later changes to
318 laser software and new hardware (pyrometer) we found the problem remains, though it is
319 much improved, and so we caution against using our current CRH data for fully
320 quantitative measurement of Arrhenius parameters at low temperatures. Note that this is
321 not a significant problem because in natural samples that are not from internal shards,
322 both alpha-ejection and diffusion profiles will lead to concave-upward Arrhenius trends at
323 low temperatures, ruling out use of these data for kinetic quantification in any case.

324 **3. Results from TAM apatite samples**

325 We analyzed 132 single apatite grains from six rocks collected from the Cathedral Rocks
326 vertical profile (Fitzgerald et al., 2006). For each apatite grain, we obtained its CRH ^4He -
327 outgassing curve, AHe age, corrected AHe age (see section 3.4), and ^4He diffusion
328 kinetics. We also use thermal histories constrained by Fitzgerald et al. (2006) from AFT
329 data to predict AHe ages using the RDAAM model, allowing us to explore any age
330 dispersion remaining after removing effects of varying radiation damage and grain size.
331 These direct results are presented in this section, and raw data for the CRH runs and U-
332 Th-Sm measurements are included in the data repository (**Table A1, A2, A3**).

333 **3.1. AHe total-gas ages and ^4He -outgassing behaviors**

334 For each of the six rock samples, at least 20 grains were analyzed by CRH, and the
335 single-grain total-gas ages were found to be highly dispersed (**Fig. 4; Fig. 5; Data**
336 **Repository – Table A1**). The intra-sample age dispersion is not surprising, given what
337 we have seen in the ages acquired by Fitzgerald et al. (2006) and the larger size of our
338 data set. Except for a few old outliers that range up to 456 ± 13 Ma, and one young outlier
339 of 6.7 ± 0.2 Ma, these apatites have ages ranging from 27.7 ± 0.9 to 165 ± 7 Ma (see
340 **Data Repository – Table A1**). We observed ^4He -outgassing curves (*df*) whose shapes
341 were nearly identical to what volume diffusion theory predicts, as well as some that were
342 anomalous compared to theoretical behavior. Anomalous ^4He -outgassing curves were
343 characterized by sharp gas-release spike(s), delayed gas-release at high temperatures,
344 or frequently a combination of both. To assist description and discussion we call apatite
345 grains having *df* curves characterized by smooth unimodal peaks as giving “expected”
346 results (i.e., they passed CRH screening), and samples showing gas spikes and high-
347 temperature release as giving “anomalous” results that failed CRH analysis.

348 All the analyzed apatites either show one or two gas-release peaks, where the early peak
349 always occurred in the range $572 \pm 45^\circ\text{C}$ (uncorrected for grain size). Less than half of
350 the apatite grains survived CRH screening for each of the six samples, and these apatites
351 have greater consistency in gas release, with the peak occurring at $590 \pm 35^\circ\text{C}$ except
352 for a few exceptions whose *df* curves were either broader or narrower than normal and/or
353 whose peak gas-release occurred at temperature ~ 50 to 100°C from the aforementioned
354 common range (**Fig. 6; Appendix A – Fig. A.2**). The apatites that survived CRH
355 screening lost at least 90% of their total ^4He between ~ 300 and 750°C , and their He ages
356 are generally younger, ranging from 30.6 ± 1.3 to 56.7 ± 1.0 Ma. The apatites that failed
357 CRH analysis show moderately or significantly anomalous ^4He -outgassing behavior, with
358 ages ranging from 33.4 ± 1.0 to >100 Ma. We also found that for each of the six samples,
359 up to seven grains that failed CRH analysis have AHe ages that are older than the AFT
360 central ages reported by Fitzgerald et al. (2006).

361 **3.2. Effects of radiation damage and grain size**

362 All of our AHe total-gas ages should be influenced by variations in radiation damage and
363 grain size to some extent. Our TAM apatite suite has a broad range from ~ 25 to 100 ppm
364 in effective uranium (hereafter eU; $[\text{eU}] = 0.238\text{Th} + 0.0012\text{Sm}$; Cooperdock et al. (2019)),
365 and F_T spherical-equivalent radii from ~ 30 to $75\ \mu\text{m}$. As in the earlier AHe single-grain
366 dataset from Cathedral Rocks (Fitzgerald et al., 2006), we found no obvious relationship
367 between measured total-gas AHe age and eU or grain size for the entire sample suite
368 (**Fig. 7C, D**). However, moderately strong age-eU and age-size relationships are evident
369 in the subset of apatites that passed CRH screening (**Fig. 7A, B**).

370 We performed forward modeling by using the thermal histories deduced from AFT data
371 (Fitzgerald et al., 2006), F_T -equivalent spherical radius, and measured eU as input for the
372 HeFTy software (Ketcham, 2005) to predict apparent ages for all of our analyzed apatites
373 by the RDAAM. We then normalized our total-gas ages to these RDAAM ages, calling the
374 resulting ratio the RDAAM-normalization (hereafter, RDN) – samples with values of 1.0
375 would have ages predicted from their eU, radius, and reference thermal history. For each
376 of the six samples, RDNs are still significantly dispersed (**Fig. 4B; Data Repository –**
377 **Table A1**) with RDN ages ranging from ~ 0.5 to 3. However, the apatites that survived
378 CRH screening show a narrower range of RDN (typically ~0.5 to 1.5), and these ranges
379 are even narrower if one looks only at RDN from the same individual samples, such as
380 R1, R2, and R6.

381 **3.3. Kinetic variations**

382 Like conventional step-heating analysis, data from CRH analysis allow for the derivation
383 of kinetic information. Using spherical geometry, cumulative fractional loss, the time
384 interval between measurements, and the average sample temperature over this interval,
385 we obtained kinetics data for ^4He diffusion for each grain.

386 We do not intend to use CRH-derived data, at least currently, for precise determination
387 of activation energy, diffusion coefficient, or closure temperature. Rather, we only explore
388 first-order intra-sample kinetic variations evident in the data. This is because: (1)
389 compared to step-heating, CRH's advantage in rapid measurement is offset at very low
390 experimental temperatures by imprecision in measurement of small gas losses, and (2)
391 temperature measurements by optical pyrometry are subject to significant systematic

392 offsets below $\sim 300^{\circ}\text{C}$ Despite our hesitation about extracting kinetic parameters from the
393 lowest-temperature portions of the Arrhenius curves, the overall locations of these curves
394 in Arrhenius space are sufficiently well defined and precise (see section 2.2.5) to allow
395 for meaningful comparisons.

396 We present only the kinetics of those apatites that passed CRH screening (**Fig. 8**), and
397 complete Arrhenius plots for all samples are supplied in Appendix A (**Fig. A.3**). We do
398 this for two reasons: First, we particularly want to explore intra-sample kinetic variations
399 between different well-behaved apatite grains. Second, owing to the fact that kinetic
400 parameters obtained from both step-heating and CRH are sensitive to fractional loss of
401 gas, any presence of gas spike(s), which mostly occurs at low to intermediate
402 temperatures, or a second high-temperature release component breaks the linearity and
403 in fact the justification for Arrhenius relationships.

404 We obtained a wide range of ^4He diffusion kinetics (**Fig. 8A**) for grains giving expected
405 results, and there is a broad correlation between their ages (total-gas age or RDN age)
406 and ^4He retentivity, as assessed by relative location on the Arrhenius plot after
407 normalizing for the effect of grain size (**Fig. 8B**) or normalizing for the collective effect of
408 grain size and eU (**Fig. 8C**). Among six samples (**Fig. 8C**), R1 and R2 show a clear
409 correlation between apparent ^4He retentivity and either total-gas age or RDN. Sample R6
410 also shows such a correlation although it does not show very much intra-sample
411 dispersion in total-gas or RDN. Kinetic data from the R6 grains show more subtle
412 variations and less spread on the Arrhenius plot relative to other samples, with the
413 exception of sample R3. Sample R3 did not show any significant intra-sample variation in

414 ^4He diffusion kinetics, while variations in both its total-gas age and RDN are significant.
415 Such correlation between age and kinetics is weaker in sample R4 and R5, unless the
416 oldest age in R4 (array of red points) and the youngest age in R5 (array of blue points)
417 are not included.

418 **3.4. Age correction**

419 We attempted to correct the ages of those apatites characterized by anomalous
420 outgassing behavior following the peak-fitting process proposed by McDannell et al.
421 (2018). Based on their assumption that gases released as spikes and at high
422 temperatures are anomalous with respect to the closure process, we started by making
423 synthetic *df* curves using established Durango kinetics and spherical geometry in order
424 to fit the first gas-release peak (i.e., low- to mid-temperature release of gas components).
425 This effectively removes gas spikes and/or delayed gas release at high temperatures (i.e.,
426 the second wave of gas release). We used the first peak because (1) the first peak is
427 almost always located at or close to the temperatures at which Durango's peak gas
428 release occurs, (2) the second peak, if present, often appears at temperatures at or above
429 those at which grains controlled by Durango kinetics have lost nearly all of their ^4He , and
430 (3) the second peaks occurred over a wide temperature range and often had broad and
431 complex shapes. We discuss the possible complexity of the delayed gas-release further
432 in **section 4**.

433 Corrected ages were calculated by stripping "extraneous" ^4He from the sample release
434 using the synthetic *df* curves as a guide, and then applying the measured U-Th-Sm.
435 Obviously, the ^4He correction will always lower ages because the correction process only

436 removes gas component(s). We found that the corrected ages of this apatite suite are
437 much younger than their total-gas counterparts, with most of them correcting to younger
438 than ca. 61 Ma, resulting in a much-reduced intra-sample dispersion (**Fig. 4; Fig. 5**).
439 However, we also noted that, for each sample, some of the corrected ages are as young
440 as ~20 Ma. This is considerably younger than the youngest ages obtained from grains
441 that passed CRH screening or other studies from the area and is probably not plausible
442 geologically (see below).

443 **4. Discussion**

444 Our results on these TAM apatites from Cathedral Rocks vertical profile revealed
445 significant intra-sample dispersion in AHe ages, and the dispersion remains even after
446 accounting for effects of grain size and eU. We found that the dispersion was significantly
447 reduced by CRH screening, and that the screened ages broadly correlate with kinetics.
448 Can these observations be reconciled by a single conceptual model? Below we relate
449 age dispersion to various types of crystal imperfections, followed by discussion of gas
450 components, complexities in age correction, and a proposed conceptual model for 4He
451 retention.

452 **4.1 Radiation damage: only one type of crystal imperfection**

453 Radiation damage, from alpha decay of U and Th, introduces imperfections in apatite
454 grains that act to slow He diffusion (e.g., Gautheron et al., 2009; Flowers et al., 2009).
455 Our results suggest that the dispersion observed in the Cathedral Rocks suite cannot be
456 explained solely by radiation damage, and therefore require the presence of a broader
457 range of crystal imperfections that add to radiation damage's role in complicating He

458 diffusion. This interpretation stems from the observation that while samples showing
459 expected diffusion behavior do exhibit possible correlations of age with grain size and eU ,
460 they also show broad correlations between age and kinetic parameters. Crystallographic
461 study also suggests that etched apatite grains from this sample suite reveal the presence
462 of dislocations and sub-grain boundaries that can potentially alter kinetic parameters (**Fig.**
463 **2**).

464 **4.2 Crystal imperfections terminology**

465 To clarify our discussion, we first define some important terms that have had various
466 usage in the (U-Th)/He literature. First, as used by Farley (2000), the term “defects” or
467 “damage” refers to a broad range of crystal imperfections stemming from thermal and
468 mechanical damage that alters the kinetics of ^4He diffusion. In U-Th/He literature the term
469 “damage” has been implicitly used as an equivalence for “radiation damage” because of
470 the development and wide application of the RDAAM model. In order to avoid
471 miscommunication, we will use “crystal defects” as an overarching term to refer to fine-
472 scale imperfections and damage resulting from deformation – dislocations, sub-grain
473 boundaries, grain boundaries and point defects (Karato, 2008), as well as radiation
474 damage; some of these defects (i.e., radiation damage) have been shown to impede
475 diffusion and have been also termed “traps”. Here we prefer to use the term “sink” to refer
476 to a broader range of probably larger imperfections such as fluid inclusions and micro-
477 voids that might act as reversible sinks for diffusing He atoms. Owing to the fact that the
478 term “trap” can depict both objects and processes, in this document we only use “trap” as
479 a verb to describe processes that temporarily “store” He atoms in reversible sinks and
480 separately use “radiation damage” when this kind of diffusion inhibition by defects is

481 mentioned. To summarize, in our usage and discussion defects are finer-scale
482 imperfections that during the diffusion random walk slow down diffusing He atoms while
483 “sinks” are larger imperfections that can physically trap He atoms and are possibly
484 reversible.

485 **4.3 Outgassing components**

486 Probably the most obvious feature of gas release from an apatite grain that fails CRH
487 screening is the delayed release of ^4He at anomalously high temperatures (above ~ 700
488 $^{\circ}\text{C}$ at a heating rate of $30^{\circ}\text{C}/\text{min}$ for typical grain sizes), which often represents a
489 considerable amount of gas and produces a second simple unimodal-like gas-release
490 peak on its df plot. This component of gas release might result from any types of crystal
491 imperfections that can act as diffusion sinks, such as fluid inclusions (Baxter, 2003), pores
492 (Lippolt et al., 1994; Watson and Cherniak, 2003; Domingos et al., 2020), and microvoids
493 (Zeitler et al., 2017). These features might trap diffusing ^4He only temporarily, in
494 proportion to the degree that these sinks are reversible. Given the low solubility of He in
495 apatite (on order 2×10^{-11} mol/g-bar; Zeitler et al., 2017), it would seem difficult for any
496 trapped He to re-enter the lattice by solution alone since the changes in pressure that
497 would accompany laboratory heating (2-3x) would be small compared to solubility
498 estimated by Henry’s-Law. It thus seems likely that an additional temperature-sensitive
499 mechanism is required to get ^4He in sinks to return to the volume-diffusion regime in the
500 lattice.

501 Another common feature of the He release from apatites that have failed CRH screening
502 is sharp spikes of gas release at low to intermediate temperatures. These spikes can at

503 times account for a considerable amount of the total ^4He release, though generally being
504 smaller compared to the ^4He released at anomalously high temperatures. These
505 characteristics suggest the presence of very near-surface crystal imperfections which can
506 rupture during heating.

507 **4.4 Evaluation of age correction**

508 Two factors make us question the age-correction procedure as we applied it. First, we
509 noted that age correction does not greatly reduce dispersion in anomalous samples, but
510 generally shifts ages to lower values that in some cases seem far too young based on
511 previous thermochronological results from this part of the TAM. Second, correction based
512 on the simple removal of ^4He released as spikes and at high temperatures implicitly relies
513 on the assumption that all these anomalous components are “extraneous” (i.e., these
514 components are not part of the syn- and post-closure radiogenic daughter production)
515 and therefore should be omitted for age calculation. However, such an assumption is
516 likely unfounded for reasons we now elaborate on.

517 **4.5 A conceptual ^4He transport model for apatite**

518 It would be ideal to have a framework that could reconcile the observed intra-sample
519 dispersion in AHe ages, anomalous outgassing components, and kinetic variations.
520 Consider an apatite that acquired a blend of crystal imperfections including both defects
521 and sinks immediately after its crystallization or perhaps later, during deformation; this
522 would almost certainly be the norm. As this apatite cooled but was still warmer than its
523 closure temperature for ^4He , during its random walk diffusing radiogenic ^4He could be
524 trapped in any larger crystal imperfections acting as sinks. The accumulation of this

525 trapped early radiogenic component would be extraneous with respect to normal
526 expectations about cooling ages. This trapping would be controlled by the density of
527 potentially many types of sinks of various sizes. In contrast, at low temperatures in nature
528 where diffusion occurs extremely slowly, there would be little or no trapping in sinks of
529 radiogenic production. Thus, natural samples would contain radiogenic ^4He in two
530 different locations: “normal” lattice sites, and sinks, with the sinks filled only with atoms
531 that had undergone significant numbers of diffusion jumps at higher temperatures. The
532 amount of ^4He in sinks would be in proportion to the number of sinks present, the ability
533 of ^4He to escape from sinks, and the thermal history, since slow cooling or isothermal
534 thermal histories will permit extended intervals over which diffusing atoms could
535 encounter a sink, in contrast to a quenched thermal history in which almost all radiogenic
536 production occurred at low temperature.

537 When laboratory outgassing is then performed, all ^4He that has not encountered a sink
538 would begin to be released through volume diffusion and this component would appear
539 in the area under the first peak of the df curve. However, atoms that are part of this “normal”
540 diffusing component would also have a high probability of encountering sinks during
541 laboratory heating. Thus, trapping could occur during two phases: for higher-temperature
542 components (i.e., at temperatures above closure) in geologic times, and for all
543 components during outgassing in the laboratory. Finally, at higher laboratory
544 temperatures, any ^4He trapped in sinks, including ^4He that was trapped both in natural
545 and in laboratory processes, would see a high probability of escaping to return to the
546 volume-diffusion regime, and be manifested in the second high-temperature release peak

547 around $\sim 800^\circ\text{C}$. In detail, given the nature of random walks in diffusion, atoms might
548 become trapped and released multiple times, depending on the kinetics of trap escape.

549 Zeitler et al. (2017) pointed out that given the large number of diffusion jumps needed for
550 an atom to escape from a crystal, the probability becomes very high that an atom will
551 encounter a feature within the lattice. This agrees with our conclusion that gas-release
552 spikes are sourced from imperfections located very near the grain surface and our
553 observation that even very badly behaved grains show only a few such spikes. The
554 number of sinks within a grain need not be very large or voluminous to significantly alter
555 diffusion systematics within a grain.

556 In this model, age correction that removes all of the laboratory high-temperature gas-
557 release would result in an underestimation of the amount of ^4He expected from closure
558 theory and therefore yield an overcorrected age. The degree of overcorrection would be
559 worst for a rapid-cooled sample in which almost all trapping happened in the laboratory,
560 and least for a sample taken directly from the partial retention zone, for which a significant
561 fraction of its ^4He found in sinks arrived there in nature.

562 What is challenging but interesting is that the ratio of low- to high-temperature gas release
563 in the laboratory is a sample-specific property that will be controlled not only by the
564 amount and type of traps, but also by the sample's thermal history. These factors will
565 determine what proportion of the sample's ^4He content was geologically mobile and thus
566 prone to trapping under natural conditions. Thus, the presence of a secondary CRH
567 release peak is most directly an indication that sink-related crystal imperfections are

568 present in the sample. Whether a useful age correction can be developed under this
569 model is unclear and will require further work. However, it is worth noting that for a given
570 sample, all of the grains will have experienced the same thermal history, therefore the
571 remaining dispersion in AHe ages after accounting for grain size and radiation damage
572 via eU suggest that other types and / or density of defects are present. An interesting
573 unanswered question is whether the presence of larger imperfections as revealed by CRH
574 would stand as a proxy for the presence of finer-scale defects that might impede diffusion
575 but not lead to trapping. This model also presents a new possibility in AHe
576 thermochronology in that the pre- and syn- closure accumulation of extraneous ^4He and
577 its laboratory release at high temperatures may offer the potential to recover additional
578 constraints on thermal history (e.g., at earlier times at higher temperatures).

579 **4.6 Kinetic variability beyond radiation-damage models**

580 CRH results from apatites that pass CRH screening shed light on first-order kinetic
581 variability of ^4He diffusion kinetics. Arrhenius plots from well-behaved grains show a
582 significant range of intra-sample kinetic variability remains after grain size and eU effects
583 are taken into account (**Fig. 8**). Additionally, while we observed some modest variations
584 in the small amounts of Si and Ce present in TAM apatites (**Section 2.2.1**), these
585 variations are not likely to lead to significant variations in the kinetics of fission-track
586 annealing, nor does variation in the Cl and OH content of these fluorapatites (Barbarand
587 et al., 2003). One might infer that this could apply to ^4He diffusion kinetics as well. The
588 published results relating apatite composition to changes in ^4He diffusivity are mixed and
589 likely complicated by the use of the FT annealing proxy Dpar. However, there is a direct
590 correlation between apatite composition and track annealing. Djimbi et al. (2015)

591 discussed calculations showing that endmember fluorapatite and chlorapatites *should*
592 have somewhat different He diffusion kinetics, however the small variation in the TAM
593 apatites suggests that halogen composition is not likely to be a significant source of the
594 kinetic variations we observed.

595 This suggests that the defects that we observed are present in varying amounts (Section
596 2.2.2) and are altering the samples' diffusion kinetics – augmenting diffusivity changes
597 due to radiation damage. This is not a surprise given how past experimental and modeling
598 studies have shown that He diffusivity in apatite is influenced by fine-scale radiation
599 damage (Flowers et al., 2009; Gautheron et al., 2009; Shuster and Farley, 2009;), with
600 pristine lattices being associated with much more rapid diffusion. Note also that in data
601 presented by Flowers et al. (2009), while radiation damage is clearly a first-order control
602 on retentivity, considerable scatter remains that we would argue reflects the presence of
603 other defects, the impacts of which would matter particularly in settings involving slow
604 cooling or thermal stagnation, where greater single-grain age dispersion often appears
605 (e.g., Reiners and Farley 2001, Fitzgerald et al., 2006).

606 **4.7 Application of CRH screening to TAM exhumation**

607 Fitzgerald et al. (2006) documented that relatively slow cooling through the late
608 Cretaceous (~1 °C/m.y.) was followed by slightly more rapid cooling (< 3 °C/m.y.) as
609 constrained by the AFT age-elevation profile and inverse thermal-history modeling, but
610 as discussed earlier, their over-dispersed AHe single-grain ages were not able to further
611 constrain the cooling/exhumation history. A final question that remains is whether after
612 extensive analysis, we are able to place better constraints on the Eocene-Oligocene

613 cooling low-temperature history for the Cathedral Rocks profile. Our samples that passed
614 screening still show considerable age dispersion, and a critical question for us is whether
615 and how to assign thermochronologically meaningful weight to each AHe age.

616 We would argue that without assessment of individual-grain diffusion kinetics, one would
617 be uncertain about the thermal history constrained by a particular AHe age. In the case
618 of our samples, the ability of CRH analysis to screen apatites based on consistent criteria
619 – unimodal *df* curves – permits us to focus on a less dispersed subset of our data. Next,
620 note that a further subset of the screened data has ⁴He diffusion kinetics similar to those
621 of Durango apatite, and all our other grains are considerably more retentive: just using
622 the offset in diffusivity seen across samples, some might be up to 25 to 30°C more
623 retentive in closure temperature than Durango apatite, meaning that their retentivity (i.e.,
624 temperature sensitivity) begins to approach that of fission tracks in apatite.

625 If we simply focus on ages from CRH-screened grains having kinetics close to Durango,
626 we do obtain better temporal constraints and evidence for a faster-cooling episode in the
627 Cenozoic (**Fig. 9, filled diamond**). This new interpretation allows us to infer that more
628 rapid rock exhumation began at or by 35-40 Ma and is quite consistent with the thermal
629 history proposed for the Peak 1880 profile on the north side of the Ferrar Glacier (**Fig. 1;**
630 **Fig. 9**) where AHe dates are less dispersed. Such increase in cooling/exhumation rate at
631 ca. 35 Ma is also a cooling/exhumation signal seen at a number of locations along the
632 TAM. This signal has been interpreted as tectonic, either due to dextral-transension
633 (Olivetti et al., 2013, 2018) or rifting and escarpment retreat further south along the
634 Transantarctic Mountain front (Miller et al. 2010). Alternatively, the timing of this enhanced

635 exhumation in the Late-Eocene-early Oligocene has been attributed to enhanced erosion
636 due to the onset of glaciation in Antarctica at ~35 Ma (e.g., He et al., 2019; Thomson et
637 al., 2019).

638 **5. Conclusions**

639 Assessment of outgassing components and evaluation of age corrections suggests that
640 ^4He transportation in apatite might be controlled by more complex models than are
641 currently being used. We argue that CRH analysis can be used to empirically screen
642 apatites for ^4He components trapped in sinks, and additionally permit assessment as to
643 whether diffusion is behaving as expected from volume diffusion and radiation-damage
644 models. In this regard, we found the youngest cluster of screened AHe ages from the
645 Cathedral Rocks in the Transantarctic Mountains, which were characterized by unimodal
646 ^4He outgassing behavior and Durango-like kinetics, suggest rapid rock exhumation at *ca.*
647 35 Ma, which is consistent with regional initiation of glaciation at the end of the Eocene
648 (ref. Ivany et al., 2006).

649 Our findings underscore the important message that simple volume diffusion and current
650 radiation-damage models may be insufficient to extract rock thermal histories for some
651 apatite populations. CRH screening analysis can characterize ^4He diffusion systematics
652 in as little as 30 minutes per aliquot, making it suitable for routine dating. Having
653 information such as this in hand before attempting age interpretations and modeling
654 seems to us far more preferable than relying on statistical manipulation or analysis of
655 numerous grains to address age dispersion after the fact. We recommend more

656 widespread deployment of CRH or $^4\text{He}/^3\text{He}$ for AHe dating, especially for sample suites
657 that show significant age dispersion.

658 **Acknowledgements**

659 Both this work and part of HG's graduate study were supported by the National Science
660 Foundation [grant EAR-1726350 to AKF, PKZ, and BDI]; PGF acknowledges support
661 from the National Science Foundation [grants OPP-0002824 and OPP-9615294] for the
662 original (U-Th)/He work along the TAM. The rock samples were originally collected as
663 part of Antarctic fieldwork through the Antarctic Research Centre of Victoria University of
664 Wellington with samples originally processed by Fitzgerald at the University of Melbourne,
665 Australia. We thank Peter Reiners, Uttam Chowdhury, and the Arizona Radiogenic Dating
666 Laboratory for U-Th-Sm-Ca measurements. Quantitative analyses were performed on a
667 JEOL JXA-8530FPlus electron microprobe at the University of Minnesota. Funding for
668 electron microprobe facility used in this research was provided by NSF under award
669 number EAR-1625422. Most graphs created using Generic Mapping Tools (GMT) v. 6.0
670 (Wessel et al., 2019).

671 **Research Data**

672 Research Data associated with this article can be accessed via Harvard Dataverse at
673 <https://doi.org/10.7910/DVN/FWAZHT>

674 **References**

- 675 Allibone A. H., Cox S. C., Graham I. J., Smellie R. W., Johnstone R. D., Ellery S. G. and
676 Palmer K. (1993) Granitoids of the Dry Valleys area, southern Victoria Land,
677 Antarctica: plutons, field relationships, and isotopic dating. *N. Z. J. Geol.*
678 *Geophys.* **36**, 281-297.
- 679 Ault A. K., Gautheron C. and King G. E. (2019) Innovations in (U–Th)/He, fission track,
680 and trapped charge thermochronometry with applications to earthquakes,
681 weathering, surface-mantle connections, and the growth and decay of
682 mountains. *Tectonics* **38**, 3705-3739.
- 683 Barbarand J., Carter A., Wood I. and Hurford T. (2003) Compositional and structural
684 control of fission-track annealing in apatite. *Chem. Geol.* **198**, 107-137.
- 685 Baxter E. F. (2003) Quantification of the factors controlling the presence of excess ⁴⁰Ar
686 or ⁴He. *Earth Planet. Sci. Lett.* **216**, 619-634.
- 687 Beucher R., Brown R. W., Roper S., Stuart F. and Persano C. (2013) Natural age
688 dispersion arising from the analysis of broken crystals: Part II. Practical application
689 to apatite (U–Th)/He thermochronometry. *Geochim. Cosmochim. Acta* **120**, 395-
690 416.
- 691 Brown R. W., Beucher R., Roper S., Persano C., Stuart F. and Fitzgerald P. (2013)
692 Natural age dispersion arising from the analysis of broken crystals. Part I:
693 Theoretical basis and implications for the apatite (U–Th)/He
694 thermochronometer. *Geochim. Cosmochim. Acta* **122**, 478-497.
- 695 Cooperdock E. H., Ketcham R. A. and Stockli D. F. (2019) Resolving the effects of 2-D
696 versus 3-D grain measurements on apatite (U–Th)/He age data and
697 reproducibility. *Geochronology* **1**, 17-41.
- 698 Dalziel I. W. (1992) Antarctica; a tale of two supercontinents? *Annu. Rev. Earth Planet.*
699 *Sci.* **20**, 501-526.
- 700 Djimbi D. M., Gautheron C., Roques J., Tassan-Got L., Gerin C. and Simoni E. (2015)
701 Impact of apatite chemical composition on (U–Th)/He thermochronometry: An
702 atomistic point of view. *Geochim. Cosmochim. Acta* **167**, 162-176.
- 703 Domingos R., Tremblay M. M., Shuster D. L. and Militzer B. (2020) Simulations and
704 Experiments Reveal Effect of Nanopores on Helium Diffusion in Quartz. *ACS Earth*
705 *Space Chem.* **4**, 1906-1912.
- 706 Farley K. A. (2000) Helium diffusion from apatite: General behavior as illustrated by
707 Durango fluorapatite. *Journal of Geophysical Research: Solid Earth* **105**, 2903-
708 2914.

- 709 Farley K. A., Wolf R. A. and Silver L. T. (1996) The effects of long alpha-stopping
710 distances on (U-Th)/He ages. *Geochim. Cosmochim. Acta* **60**, 4223-4229.
- 711 Farley K. A. (2002) (U-Th)/He dating: Techniques, calibrations, and
712 applications. *Reviews in Mineralogy and Geochemistry* **47**, 819-844.
- 713 Fitzgerald P. G., Baldwin S. L., Webb L. E. and O'Sullivan P. B. (2006) Interpretation of
714 (U-Th)/He single grain ages from slowly cooled crustal terranes: a case study from
715 the Transantarctic Mountains of southern Victoria Land. *Chem. Geol.* **225**, 91-120.
- 716 Florindo F., Wilson G. S., Roberts A. P., Sagnotti L. and Verosub K. L. (2001)
717 Magnetostratigraphy of late Eocene-early Oligocene strata from the CRP-3 core,
718 Victoria Land Basin, Antarctica. *Terra Antartica* **8**, 599-614.
- 719 Flowers R. M. and Farley K. A. (2012) Apatite $^4\text{He}/^3\text{He}$ and (U-Th)/He evidence for an
720 ancient Grand Canyon. *Science* **338**, 1616-1619.
- 721 Flowers R. M. and Kelley S. A. (2011) Interpreting data dispersion and "inverted" dates
722 in apatite (U-Th)/He and fission-track datasets: an example from the US
723 midcontinent. *Geochim. Cosmochim. Acta* **75**, 5169-5186.
- 724 Flowers R. M., Ketcham R. A., Shuster D. L. and Farley K. A. (2009) Apatite (U-Th)/He
725 thermochronometry using a radiation damage accumulation and annealing
726 model. *Geochim. Cosmochim. Acta* **73**, 2347-2365.
- 727 Galeotti S., DeConto R., Naish T., Stocchi P., Florindo F., Pagani M., Barrett P., Bohaty
728 S. M., Lanci L. and Pollard D. (2016) Antarctic Ice Sheet variability across the
729 Eocene-Oligocene boundary climate transition. *Science* **352**, 76-80.
- 730 Gautheron C., Tassan-Got L., Barbarand J. and Pagel M. (2009) Effect of alpha-
731 damage annealing on apatite (U-Th)/He thermochronology. *Chem. Geol.* **266**, 157-
732 170.
- 733 Gerin C., Gautheron C., Oliviero E., Bachelet C., Djimbi D. M., Seydoux-Guillaume A.,
734 Tassan-Got L., Sarda P., Roques J. and Garrido F. (2017) Influence of vacancy
735 damage on He diffusion in apatite, investigated at atomic to mineralogical
736 scales. *Geochim. Cosmochim. Acta* **197**, 87-103.
- 737 Goodge J. W. (2020) Geological and tectonic evolution of the Transantarctic Mountains,
738 from ancient craton to recent enigma. *Gondwana Research* **80**, 50-122.
- 739 Green P. and Duddy I. (2018) Apatite (U-Th-Sm)/He thermochronology on the wrong
740 side of the tracks. *Chem. Geol.* **488**, 21-33.
- 741 Gunn B. M. and Warren G. (1962) *Geology of Victoria Land between the Mawson and*
742 *Mulock Glaciers, Antarctica*. Trans-Antarctic Expedition Committee,
- 743 He J., Thomson S. N. and Reiners P. W. (2019) Apatite (U-Th)/He thermochronometric
744 data show rapid late Eocene incision in the central Transantarctic Mountains. *AGU*
745 *Fall Meeting*, C53B-1340.

- 746 Idleman B. D., Zeitler P. K. and McDannell K. T. (2018) Characterization of helium
747 release from apatite by continuous ramped heating. *Chem. Geol.* **476**, 223-232.
- 748 Ivany L. C., Van Simaeys S., Domack E. W. and Samson S. D. (2006) Evidence for an
749 earliest Oligocene ice sheet on the Antarctic Peninsula. *Geology* **34**, 377-380.
- 750 Karato S. (2008) *Deformation of Earth Materials: An Introduction to the Rheology of*
751 *Solid Earth*. Cambridge University Press, Cambridge.
- 752 Ketcham R. A., Carter A., Donelick R. A., Barbarand J. and Hurford A. J. (2007)
753 Improved modeling of fission-track annealing in apatite. *Am. Mineral.* **92**, 799-810.
- 754 Ketcham R. A., Gautheron C. and Tassan-Got L. (2011) Accounting for long alpha-
755 particle stopping distances in (U-Th-Sm)/He geochronology: refinement of the
756 baseline case. *Geochim. Cosmochim. Acta* **75**, 7779-7791.
- 757 Krogh T. E. (1982) Improved accuracy of U-Pb zircon ages by the creation of more
758 concordant systems using an air abrasion technique. *Geochim. Cosmochim.*
759 *Acta* **46**, 637-649.
- 760 Lippolt H. J., Leitz M., Wernicke R. S. and Hagedorn B. (1994) (Uranium
761 thorium)/helium dating of apatite: experience with samples from different
762 geochemical environments. *Chem. Geol.* **112**, 179-191.
- 763 Long S. P., Thomson S. N., Reiners P. W. and Di Fiori R. V. (2015) Synorogenic
764 extension localized by upper-crustal thickening: An example from the Late
765 Cretaceous Nevadaplano. *Geology* **43**, 351-354.
- 766 McDannell K. T., Zeitler P. K., Janes D. G., Idleman B. D. and Fayon A. K. (2018)
767 Screening apatites for (U-Th)/He thermochronometry via continuous ramped
768 heating: He age components and implications for age dispersion. *Geochim.*
769 *Cosmochim. Acta* **223**, 90-106.
- 770 McDowell F. W., McIntosh W. C. and Farley K. A. (2005) A precise ^{40}Ar - ^{39}Ar reference
771 age for the Durango apatite (U-Th)/He and fission-track dating standard. *Chem.*
772 *Geol.* **214**, 249-263.
- 773 Meesters A. and Dunai T. J. (2002) Solving the production-diffusion equation for finite
774 diffusion domains of various shapes: Part II. Application to cases with α -ejection
775 and nonhomogeneous distribution of the source. *Chem. Geol.* **186**, 57-73.
- 776 Murray K. E., Orme D. A. and Reiners P. W. (2014) Effects of U-Th-rich grain boundary
777 phases on apatite helium ages. *Chem. Geol.* **390**, 135-151.
- 778 Peyton S. L., Reiners P. W., Carrapa B. and DeCelles P. G. (2012) Low-temperature
779 thermochronology of the northern Rocky Mountains, western USA. *Am. J.*
780 *Sci.* **312**, 145-212.
- 781 Piccoli P. M. and Candela P. A. (2002) Apatite in igneous systems. *Reviews in*
782 *Mineralogy and Geochemistry* **48**, 255-292.

- 783 Reiners P. W., Ehlers T. A., Mitchell S. G. and Montgomery D. R. (2003) Coupled
784 spatial variations in precipitation and long-term erosion rates across the
785 Washington Cascades. *Nature* **426**, 645-647.
- 786 Reiners P. W., Ehlers T. A. and Zeitler P. K. (2005) Past, present, and future of
787 thermochronology. *Reviews in Mineralogy and Geochemistry* **58**, 1-18.
- 788 Reiners P. W. and Farley K. A. (2001) Influence of crystal size on apatite (U–Th)/He
789 thermochronology: an example from the Bighorn Mountains, Wyoming. *Earth
790 Planet. Sci. Lett.* **188**, 413-420.
- 791 Shuster D. L., Flowers R. M. and Farley K. A. (2006) The influence of natural radiation
792 damage on helium diffusion kinetics in apatite. *Earth Planet. Sci. Lett.* **249**, 148-
793 161.
- 794 Shuster D. L. and Farley K. A. (2009) The influence of artificial radiation damage and
795 thermal annealing on helium diffusion kinetics in apatite. *Geochim. Cosmochim.
796 Acta* **73**, 183-196.
- 797 Smellie J. L. (2001) History of Oligocene erosion, uplift and unroofing of the
798 Transantarctic Mountains deduced from sandstone detrital modes in CRP-3
799 drillcore, Victoria Land Basin, Antarctica. *Terra Antartica* **8**, 481-490.
- 800 Spiegel C., Kohn B., Belton D., Berner Z. and Gleadow A. (2009) Apatite (U–Th–
801 Sm)/He thermochronology of rapidly cooled samples: the effect of He
802 implantation. *Earth Planet. Sci. Lett.* **285**, 105-114.
- 803 Thomson S. N., Reiners P. W., He J., Hemming S. R. and Licht K. (2019) New
804 constraints on the pre-glacial and glacial uplift and incision history of the central
805 Transantarctic Mountains using multiple low-temperature
806 thermochronometers. *AGU Fall Meeting*, C14B-04.
- 807 Toraman E., Teyssier C., Whitney D. L., Fayon A. K., Thomson S. N. and Reiners P. W.
808 (2014) Low-temperature thermochronologic record of Eocene migmatite dome
809 emplacement and late Cenozoic landscape development, Shuswap core complex,
810 British Columbia. *Tectonics* **33**, 1616-1635.
- 811 Watson E. B. and Cherniak D. J. (2003) Lattice diffusion of Ar in quartz, with constraints
812 on Ar solubility and evidence of nanopores. *Geochim. Cosmochim. Acta* **67**, 2043-
813 2062.
- 814 Wessel P., Luis J. F., Uieda L., Scharroo R., Wobbe F., Smith W. and Tian D. (2019)
815 The generic mapping tools version 6. *Geochem. Geophys. Geosyst.* **20**, 5556-5564.
- 816 Willett C. D., Fox M. and Shuster D. L. (2017) A helium-based model for the effects of
817 radiation damage annealing on helium diffusion kinetics in apatite. *Earth Planet.
818 Sci. Lett.* **477**, 195-204.
- 819 Wilson G. S., Roberts A. P., Verosub K. L., Florindo F. and Sagnotti L. (1998)
820 Magnetobiostratigraphic chronology of the Eocene—Oligocene transition in the

- 821 CIROS-1 core, Victoria Land margin, Antarctica: Implications for Antarctic glacial
822 history. *Geological Society of America Bulletin* **110**, 35-47.
- 823 Wolf R. A., Farley K. A. and Silver L. T. (1996) Helium diffusion and low-temperature
824 thermochronometry of apatite. *Geochim. Cosmochim. Acta* **60**, 4231-4240.
- 825 Zeitler P. K., Herczeg A. L., McDougall I. and Honda M. (1987) U-Th-He dating of
826 apatite: A potential thermochronometer. *Geochim. Cosmochim. Acta* **51**, 2865-
827 2868.
- 828 Zeitler, P., Brown R. and Hackspacher P. (2017), Better tools for tracing the thermal
829 history of rocks. *Eos* **98**, doi:10.1029/2017EO073479.
- 830 Zeitler P. K., Enkelmann E., Thomas J. B., Watson E. B., Ancuta L. D. and Idleman B.
831 D. (2017) Solubility and trapping of helium in apatite. *Geochim. Cosmochim.*
832 *Acta* **209**, 1-8.

833 **Figure Captions**

834 **Figure 1.** (A) Simplified map of southern Victoria Land showing location of the two vertical
835 sampling profiles from Peak 1880 and Cathedral Rocks. Filled areas are ice free. TAM:
836 Transantarctic Mountains. (B and C) Composite AFT and AHe plots summarizing the
837 preferred cooling/exhumation path (dashed line) for the two vertical profiles but with AHe
838 data moved down in elevation relative to the AFT data based on the difference in closure
839 temperatures (30 – 35 °C) divided by the estimated paleogeothermal gradient (20 –
840 35 °C/km). Modified from Fitzgerald et al. (2006). For the AHe data, Fitzgerald et al. (2006)
841 judged that younger AHe ages (between the minimum age and a weighted mean) were
842 more likely to constrain a “true” thermal history, perhaps an early precursor to using
843 screened CRH-screened ages (as shown in this study, section 4.7). Less dispersion in
844 the Peak 1880 AHe data allowed constraints to be placed on Late Eocene cooling,
845 whereas much greater dispersion in AHe data from Cathedral Rocks precluded such
846 constraints.

847 **Figure 3.** Incremental ⁴He release (*df*) curves (A), and CRH-derived Arrhenius
848 relationships (B) of Durango apatites under a 30 °C/min heating ramp rate. Gray curves
849 and circles depict result from Durango shards; blue curves and triangles show result from
850 Durango balls. Red dashed line marks diffusion kinetics of ⁴He in Durango apatite
851 acquired by Farley (2000) via step-heating, adjusted to a radius of 80 μm. (C) Arrhenius
852 plot of the same analyses adjusted to a common spherical-equivalent radius of *a* = 80 μm
853 in order to assess precision in the kinetics obtained by CRH, an indirect verification of
854 temperature control. (D) shows the temperature uncertainties at two points for CRH
855 analysis of Durango balls.

856 **Figure 4.** Single-grain AHe ages (upper plot) and RDAAM-normalized relative ages
857 (lower plot). Ages from each sample are presented in individual panels. Each plot includes
858 measured single-grain total-gas age, screened age, and CRH-corrected age,
859 accompanied by their kernel density estimations (KDEs). For better visualization ages
860 older than 100 Ma were omitted; Table A1 shows information for all ages.

861 **Figure 5.** Cathedral Rocks AHe and AFT age-elevation plots summarizing results and
862 interpretations from this study and from Fitzgerald et al. (2006). Light blue circles and
863 curves show single-grain total-gas AHe ages (this study) and their KDE, respectively;
864 dark blue circles and shaded curves show single-grain screened AHe ages (this study)
865 and their KDE; pink shaded curves show KDE of single-grain CRH-corrected ages; red
866 circles show AHe weighed mean ages (Fitzgerald et al., 2006); orange triangles show
867 AFT central ages (Fitzgerald et al., 2006); red dashed line shows best-fit trend to the
868 weighted mean AHe ages from Fitzgerald et al. (2006).

869 **Figure 6.** *df* curves measured using a 30 °C/min ramped heating schedule. Results from
870 each sample are presented in individual subpanels. (A) Results from grains that passed
871 CRH screening. (B) Results from grains that failed screening. (C) Results from all grains,
872 color-coded into three groups: blue, grains whose AHe ages are not older than the oldest
873 screened age in that sample; red, grains whose AHe ages are older than the fission-track
874 central ages measured by Fitzgerald et al. (2006); orange, grains whose ages fall
875 between the other two groups.

876 **Figure 7.** (A) Relationships between single-grain AHe age and grain size (total
877 compilation shown in panel C). (B) Relationships between single-grain AHe age and
878 equivalent uranium (eU) (total compilation shown in panel D). Sizes are calculated as F_T
879 -equivalent spherical radius. To be consistent with prior publications eU is calculated as
880 $U + 0.235 \cdot Th$; Cooperdock et al (2019) provide a more accurate update). Filled circles
881 show grains that passed CRH screening.

882 **Figure 8.** CRH-derived Arrhenius relationships of apatite grains that passed CRH
883 screening, showing relationship between AHe ages and apparent ^4He diffusivity. (A)
884 Observed kinetics color-coded by observed age. (B) Kinetics adjusted to 80 μm radius,
885 color-coded by observed age. (C) Kinetics adjusted to 80 μm radius, color-coded by
886 RDAAM-normalized relative age. Dashed green line show the kinetics of ^4He diffusion in
887 Durango apatites measured by Farley (2000). Vertical dotted line provides visual
888 reference to aid comparison of diffusivity variations at $10000/K = 15$ (~ 393.5 °C).

889 **Figure 9.** Composite AFT and AHe plot (constructed as Figure 1C) summarizing our
890 updated cooling/exhumation path for the Cathedral Rocks locality. Preferred path for
891 Peak 1880 is from Fitzgerald et al. (2006).

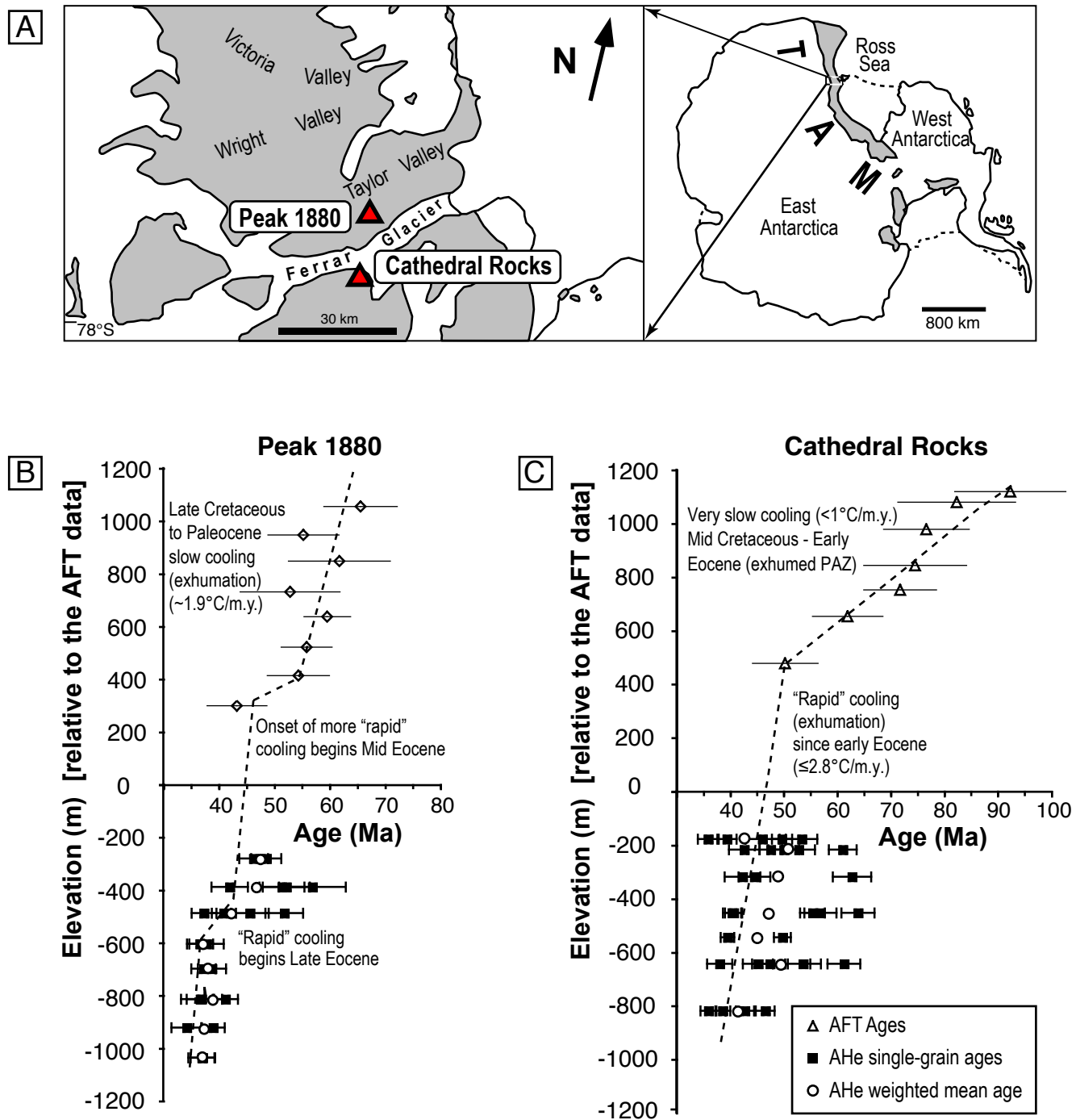


Figure. 1

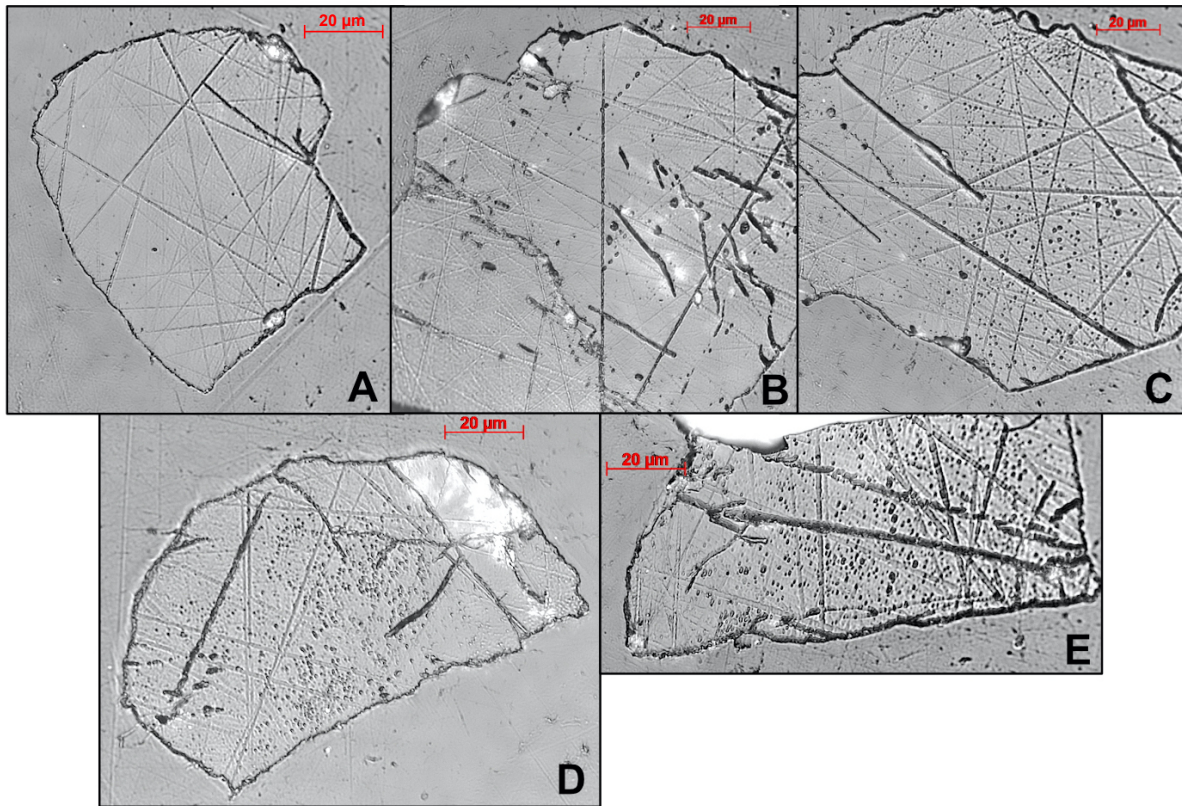


Figure 2

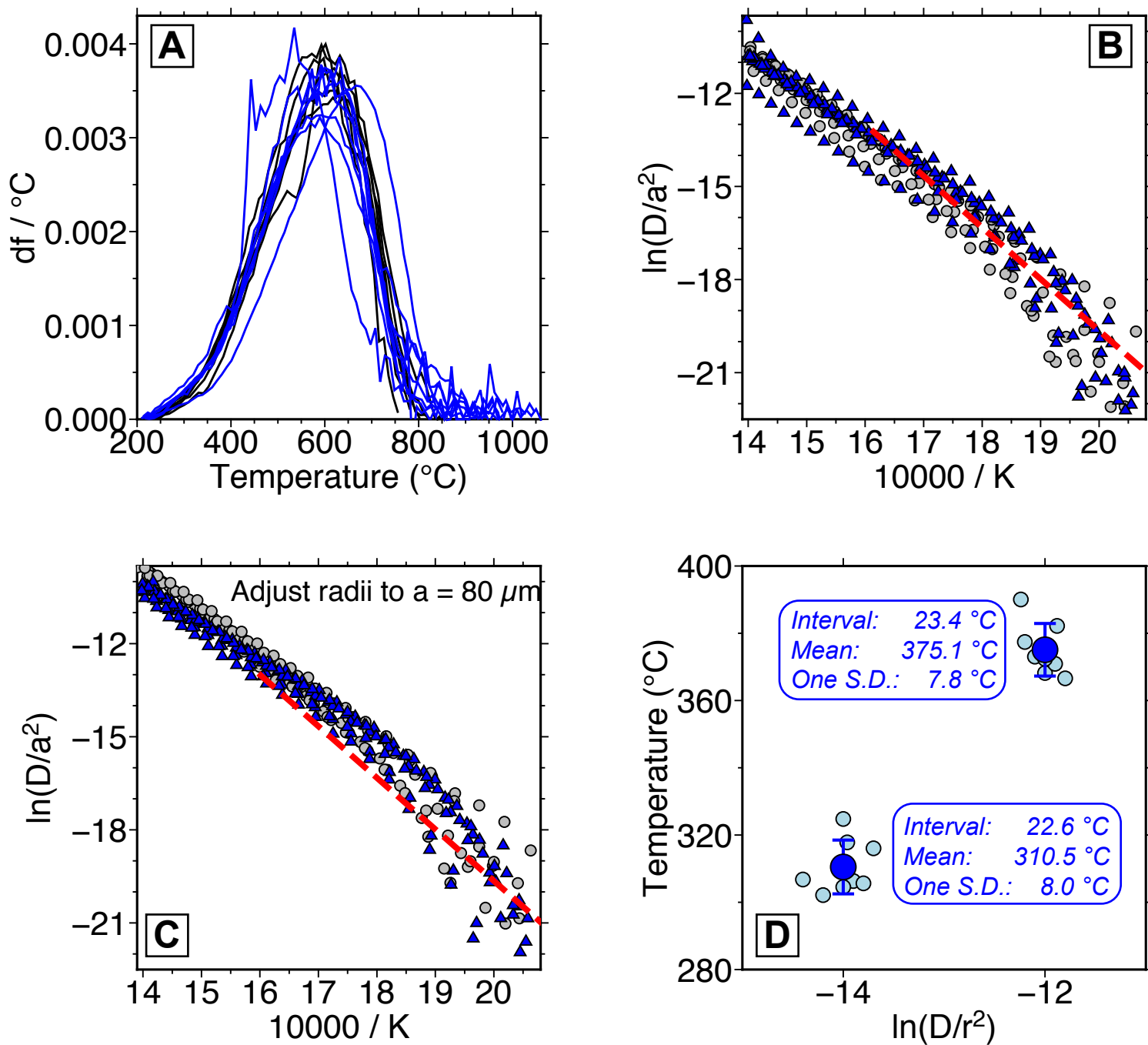


Figure 3

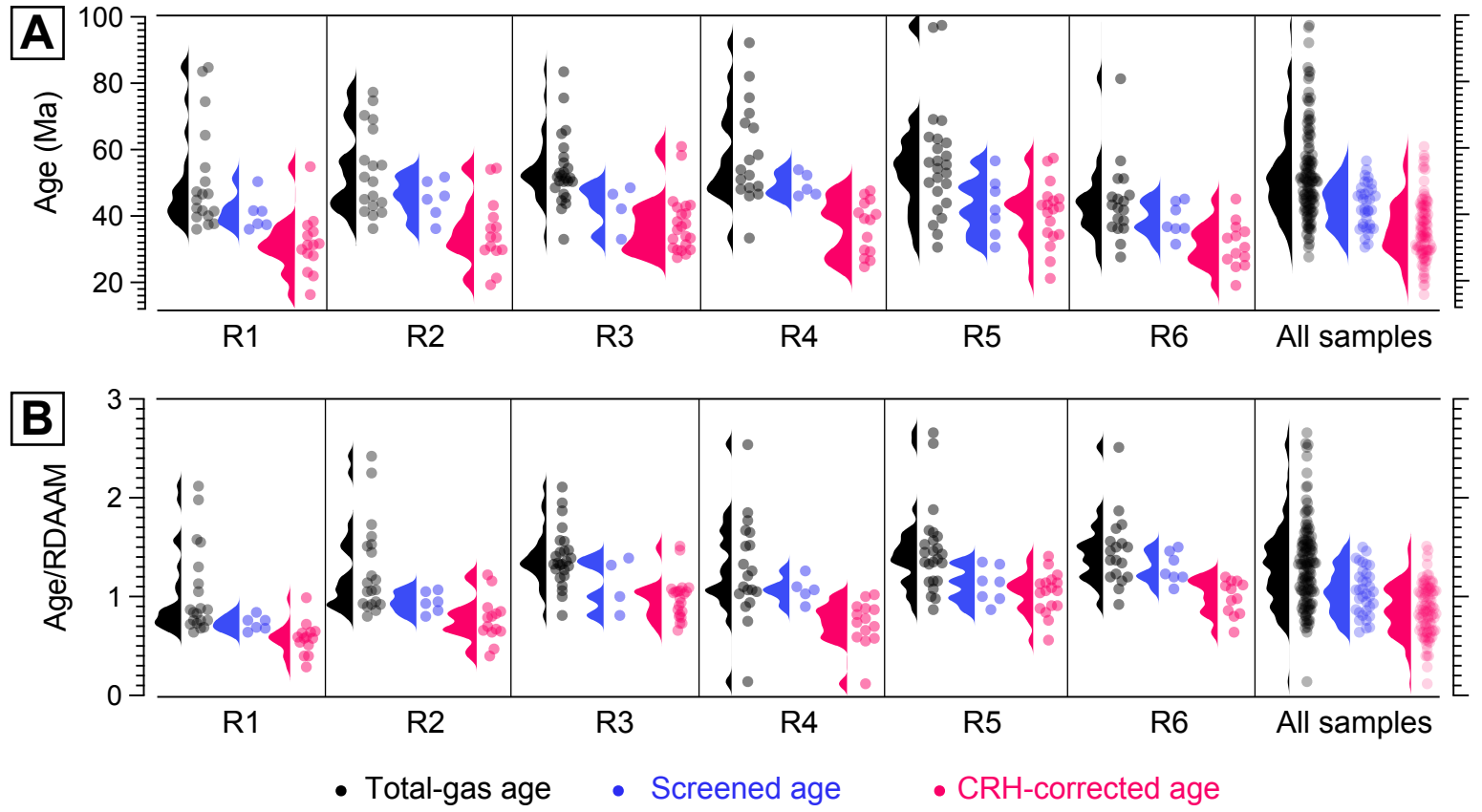


Figure 4

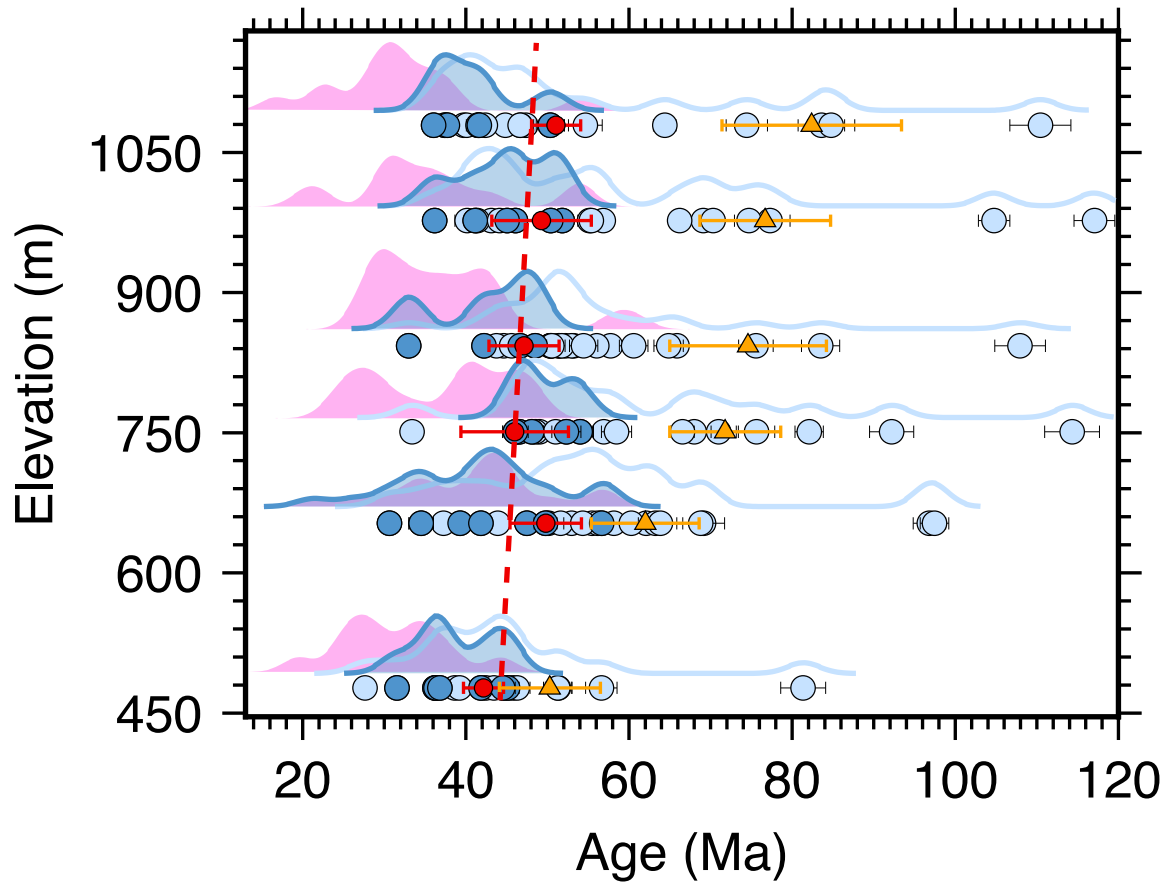


Figure 5

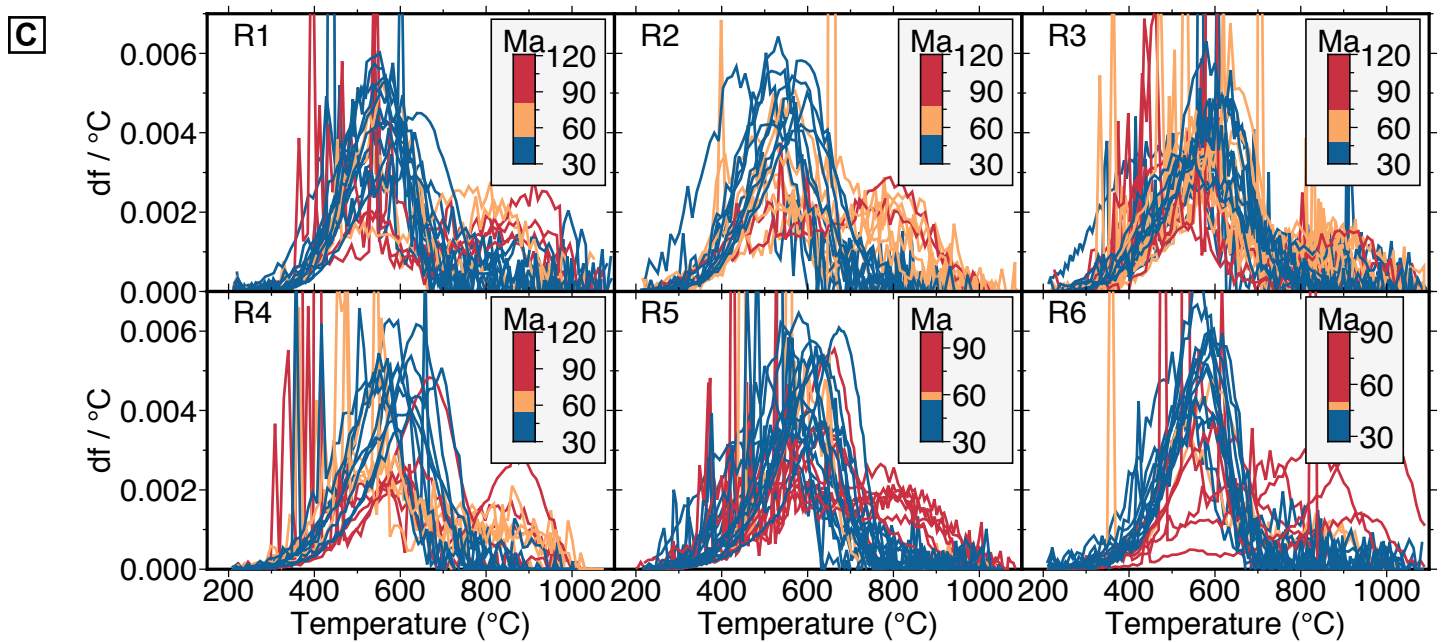
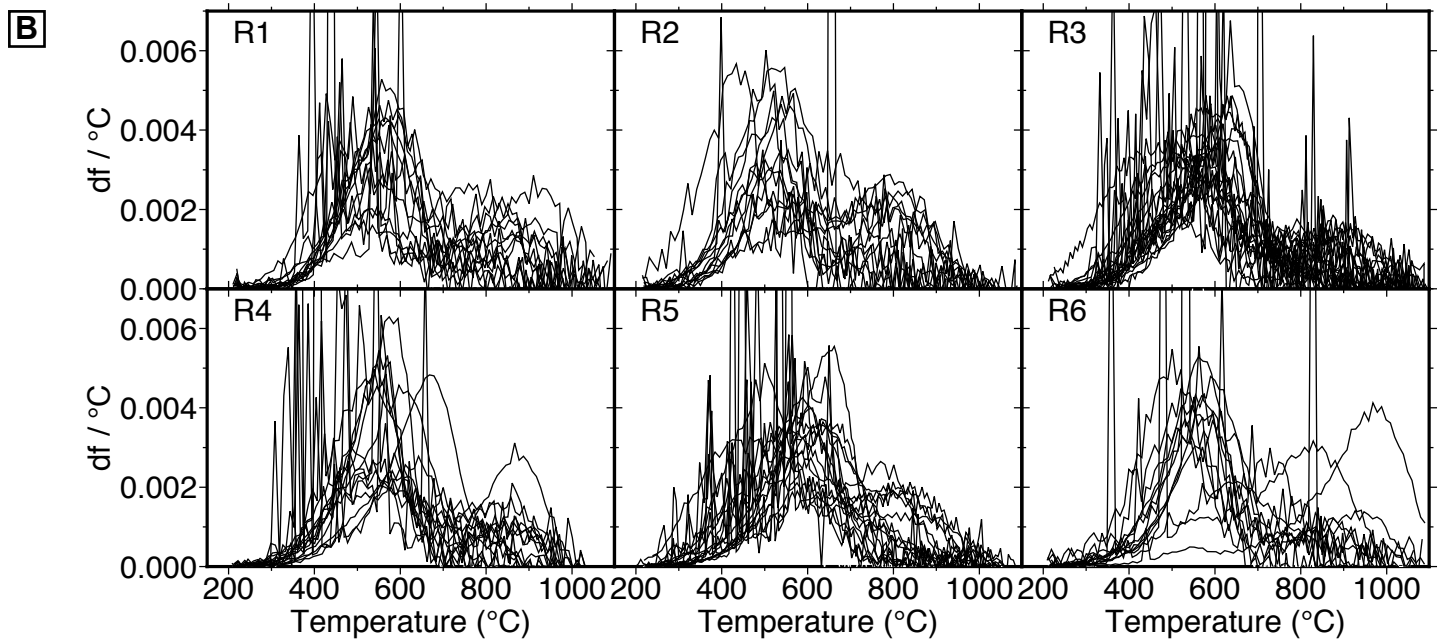
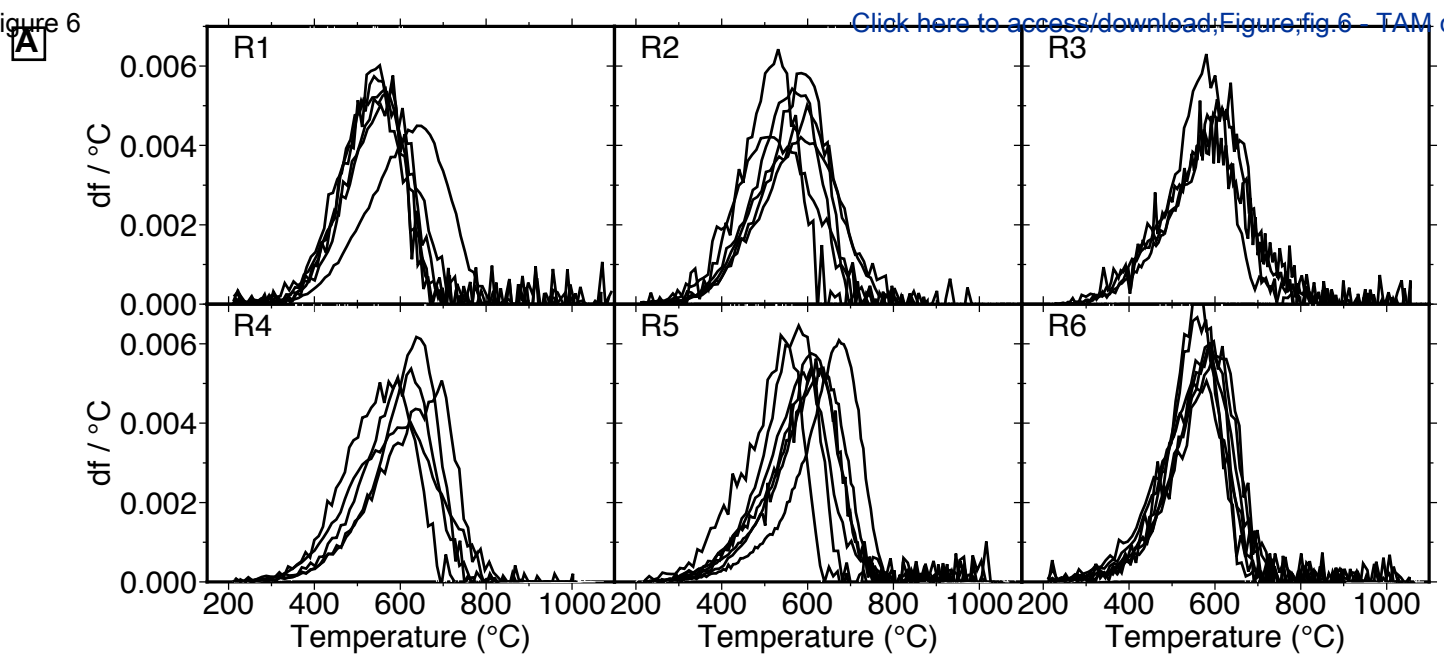


Figure 6

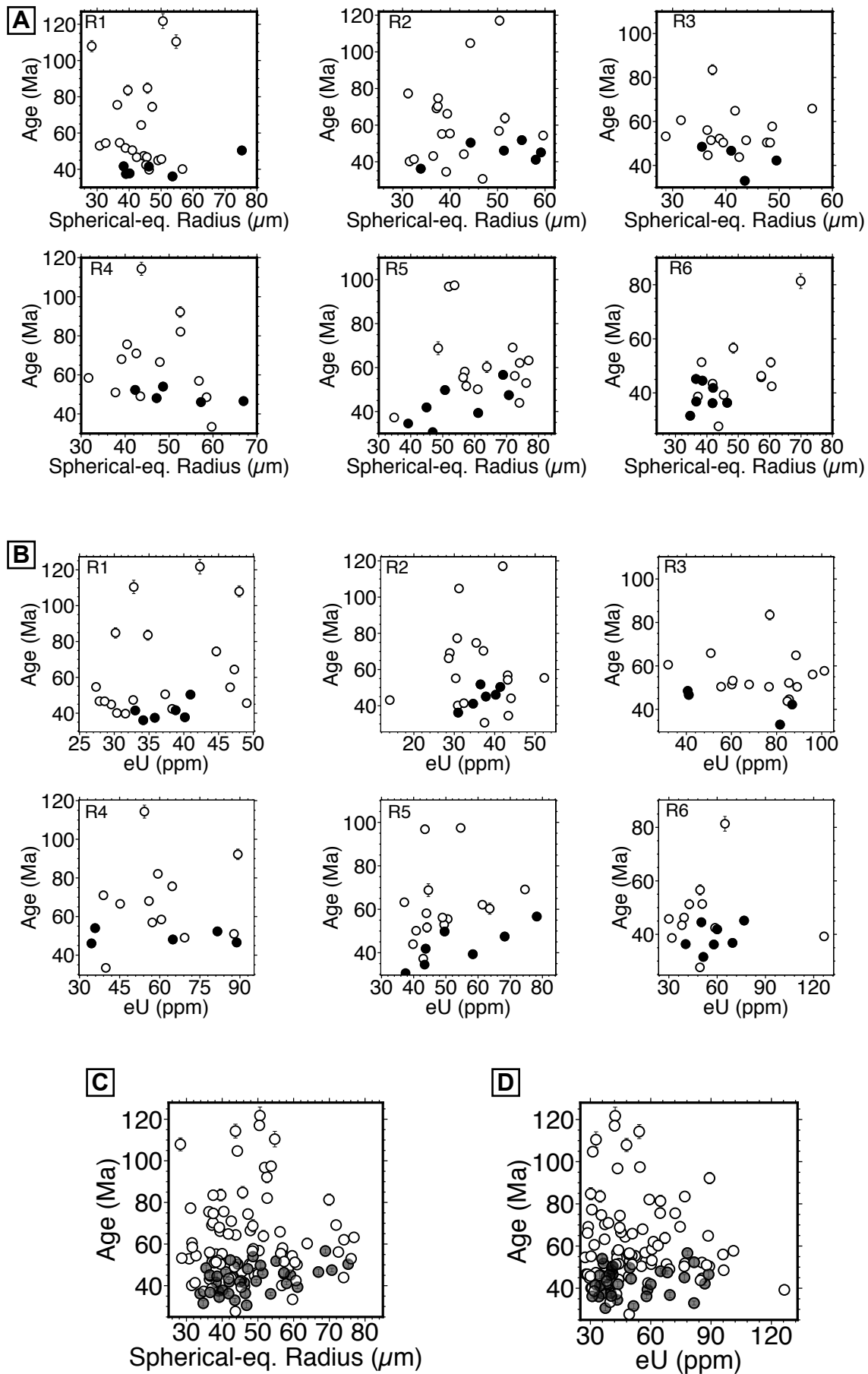


Figure 7

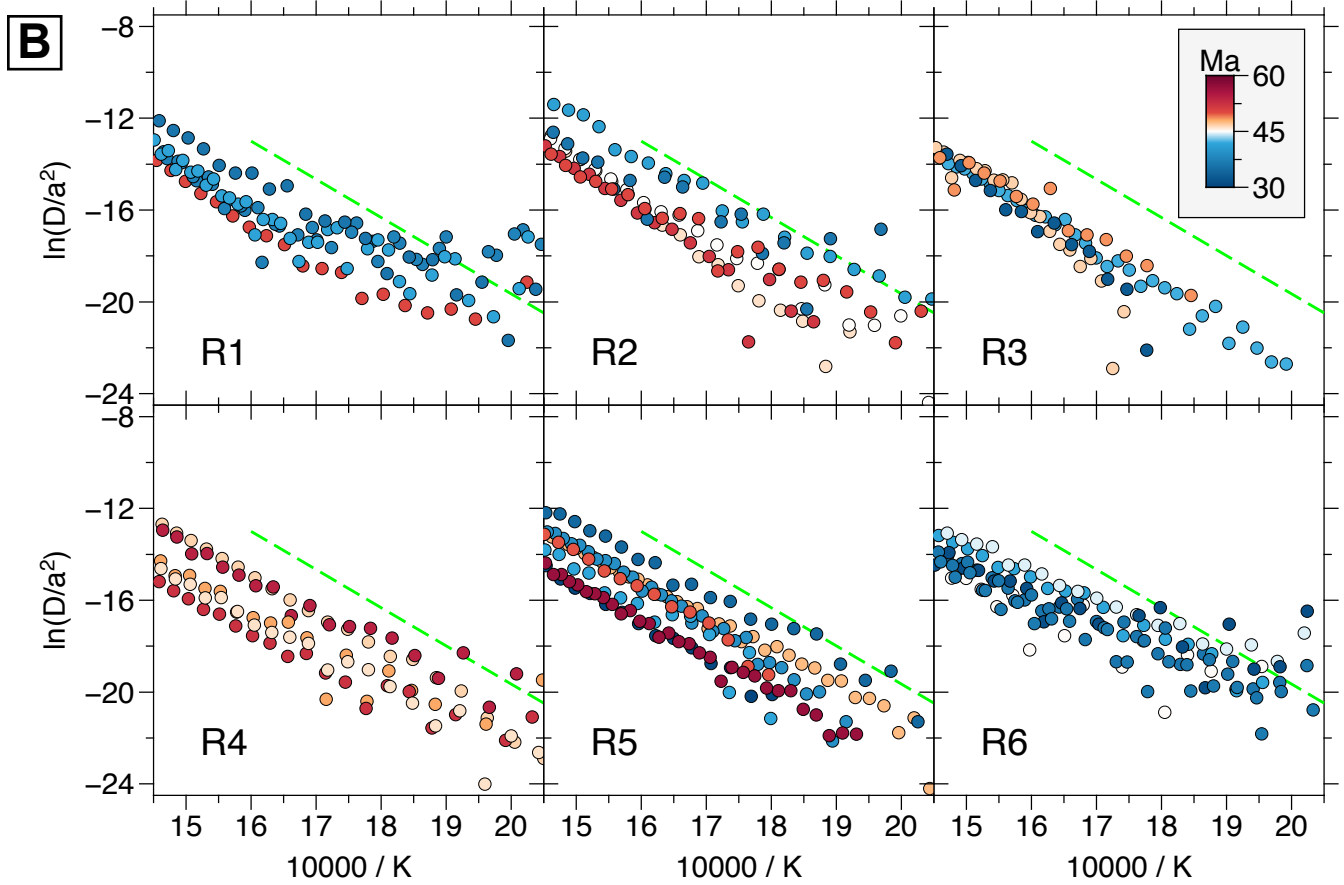
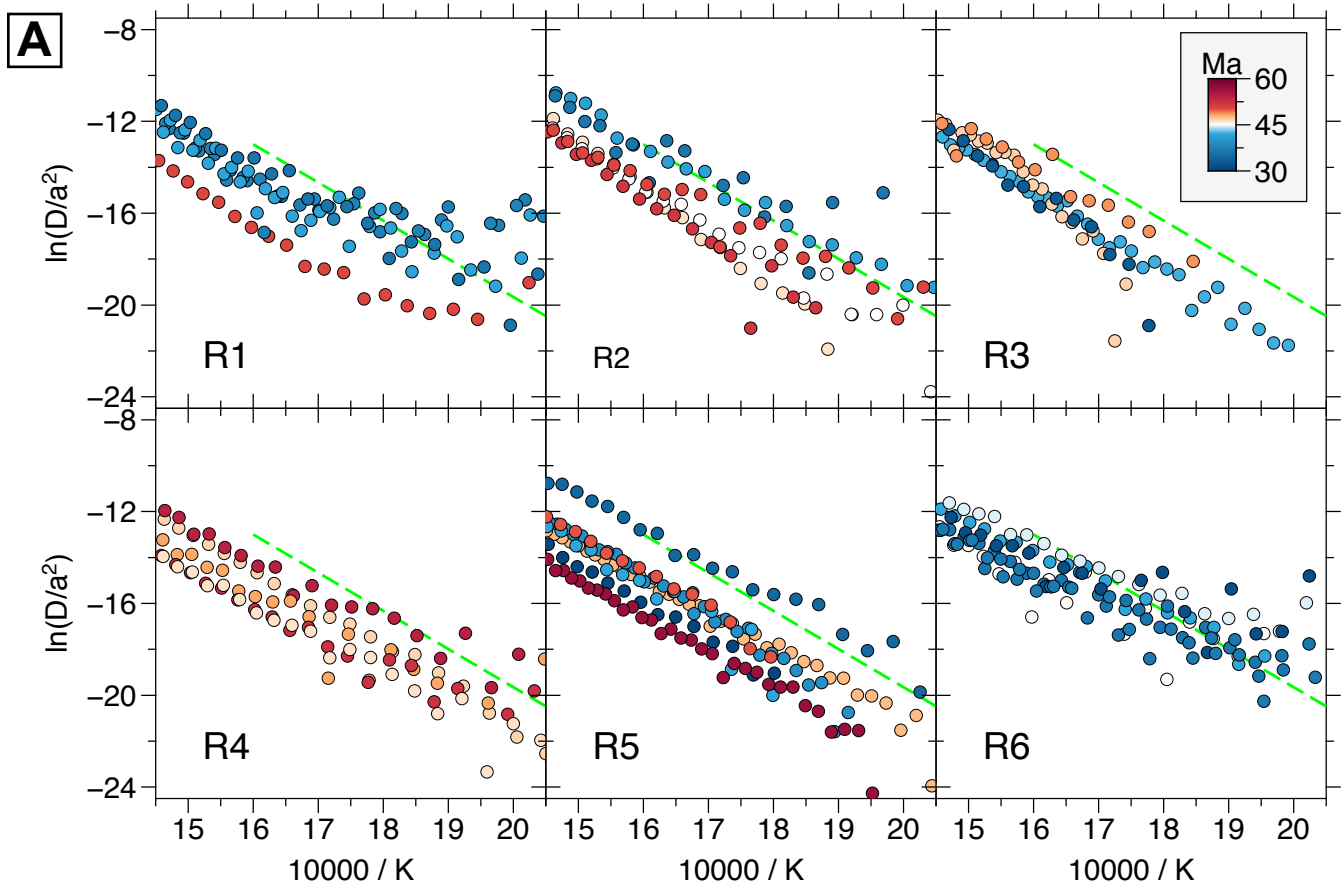


Figure 8

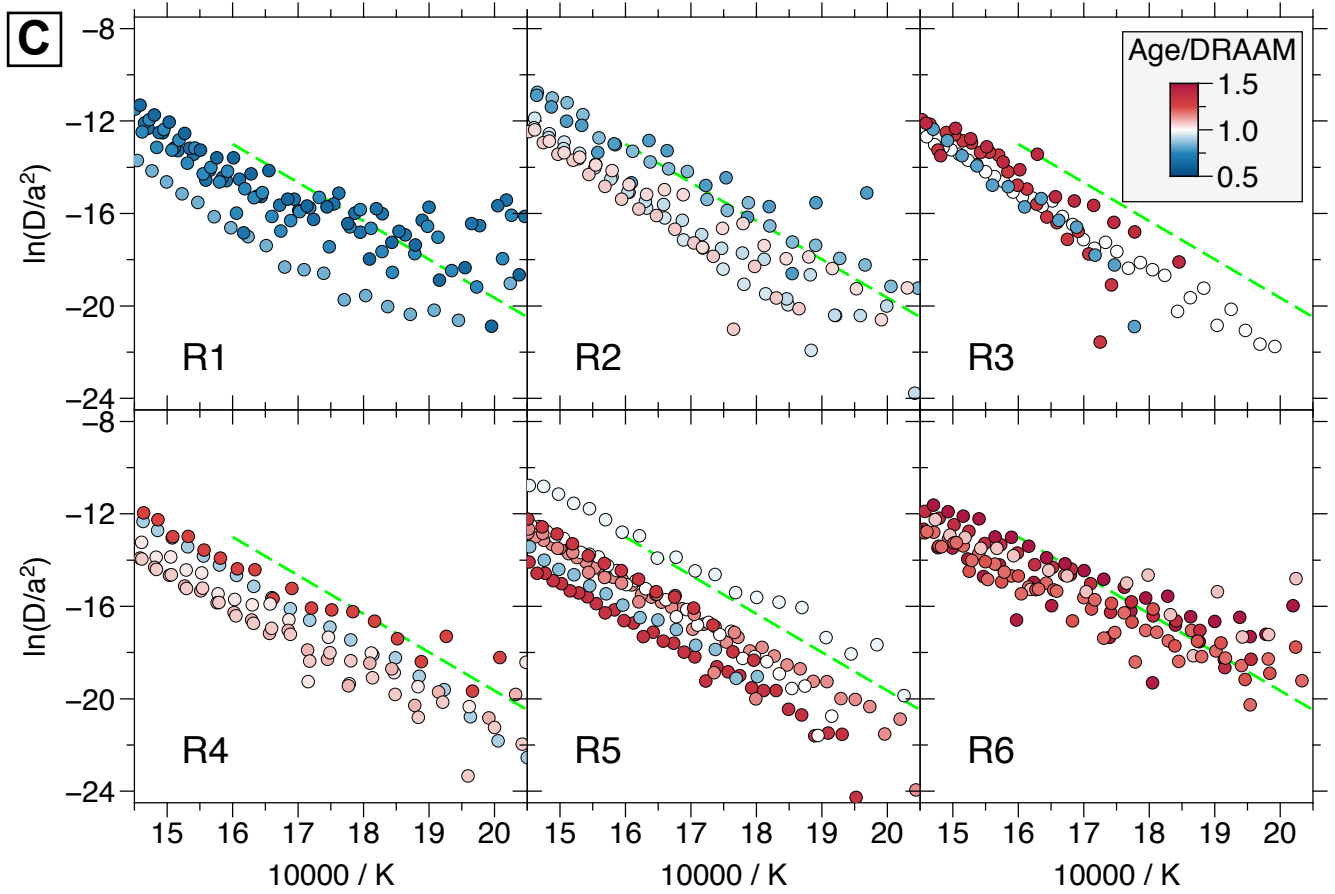


Figure 8 - continued

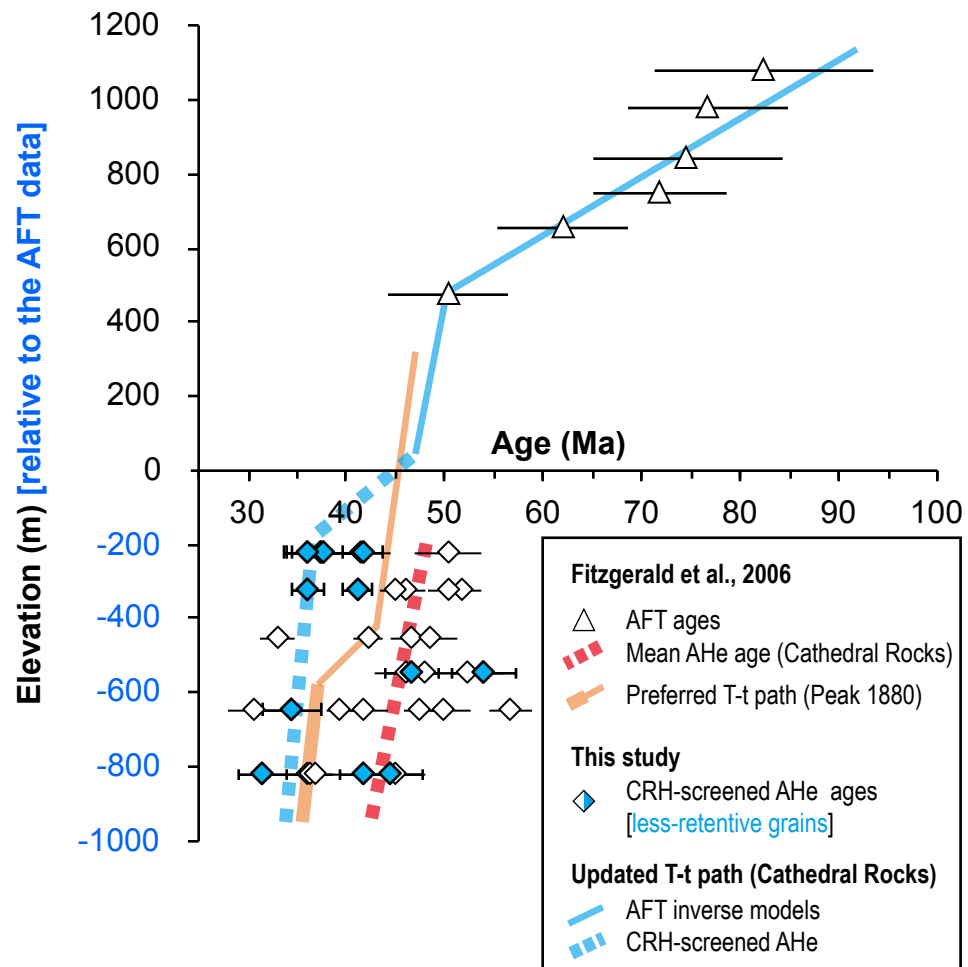
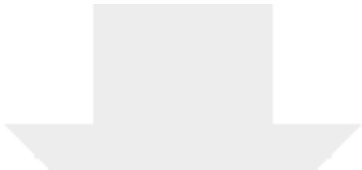
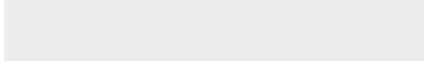
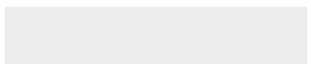


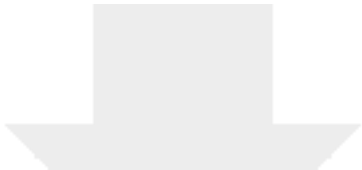
Figure 9



Click here to access/download

Appendix
Appendix_A.pdf





Click here to access/download

Appendix
Appendix_B.pdf

